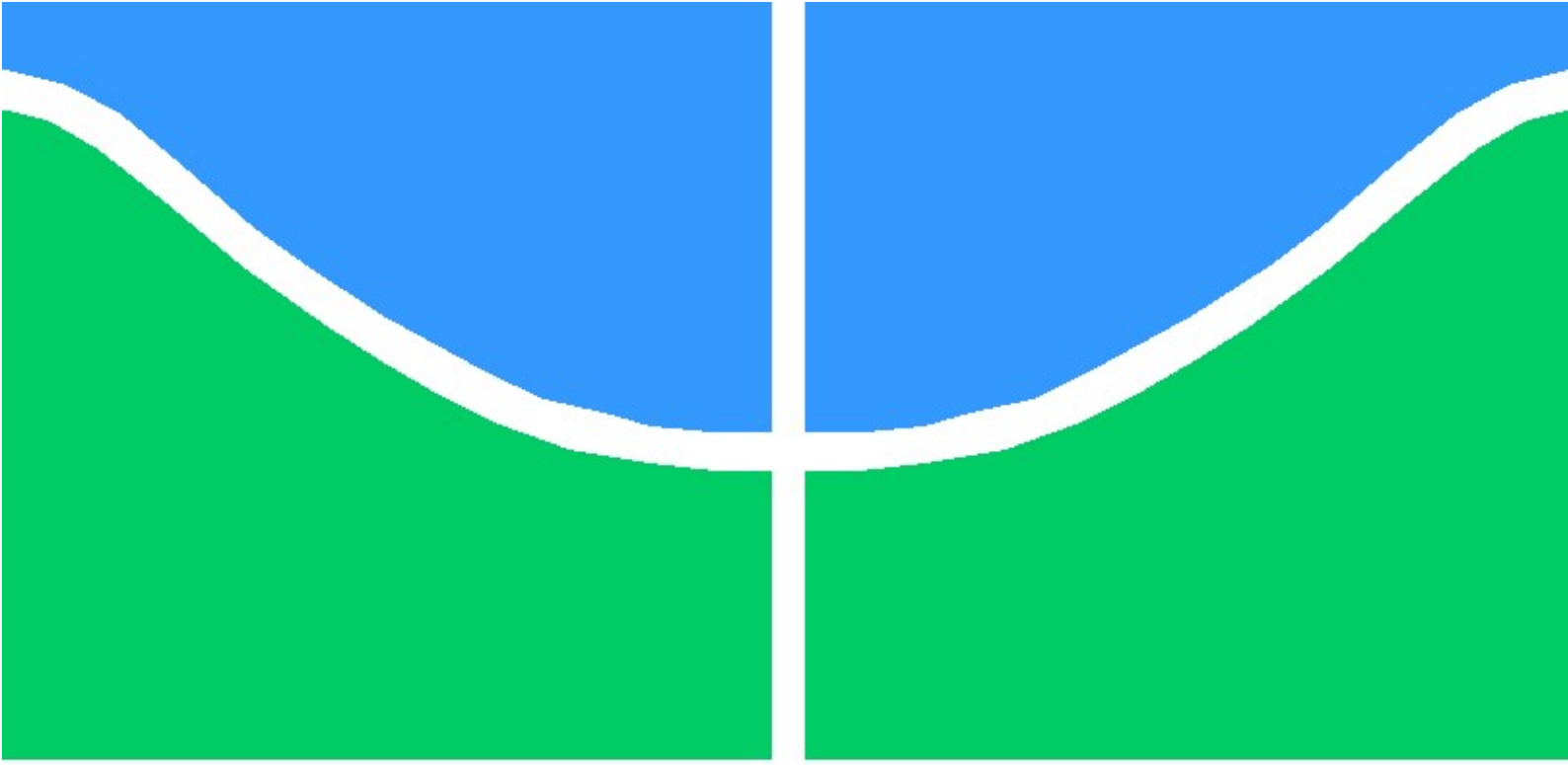

Evaluation of Amazonian Wood Residue Blends for Decentralized Energy Recovery: Combustion Parameters and Potential Emissions.

MAYARA GABI MOREIRA

DISSERTAÇÃO DE MESTRADO EM CIÊNCIAS MECÂNICAS
DEPARTAMENTO DE ENGENHARIA MECÂNICA

FACULDADE DE TECNOLOGIA
UNIVERSIDADE DE BRASÍLIA

UNIVERSIDADE DE BRASÍLIA
FACULDADE DE TECNOLOGIA
DEPARTAMENTO DE ENGENHARIA MECÂNICA
PROGRAMA DE PÓS-GRADUAÇÃO EM CIÊNCIAS MECÂNICAS

EVALUATION OF AMAZONIAN WOOD RESIDUE BLENDS FOR DECENTRALIZED ENERGY RECOVERY: COMBUSTION PARAMETERS AND POTENTIAL EMISSIONS

MAYARA GABI MOREIRA

Orientador: PROF. DR. EDGAR AMARAL SILVEIRA, ENM/UNB

DISSERTAÇÃO DE MESTRADO EM ENGENHARIA MECÂNICA

BRASÍLIA-DF, 27 DE FEV DE 2025

UNIVERSIDADE DE BRASÍLIA
FACULDADE DE TECNOLOGIA
DEPARTAMENTO DE ENGENHARIA MECÂNICA
PROGRAMA DE PÓS-GRADUAÇÃO EM CIÊNCIAS MECÂNICAS

AVALIAÇÃO DE MISTURAS DE RESÍDUOS DE MADEIRA AMAZÔNICA PARA RECUPERAÇÃO DE ENERGIA DESCENTRALIZADA: PARÂMETROS DE COMBUSTÃO E POTENCIAL DE EMISSÕES

MAYARA GABI MOREIRA

Orientador: PROF. DR. EDGAR AMARAL SILVEIRA, ENM/UNB

DISSERTAÇÃO DE MESTRADO EM ENGENHARIA MECÂNICA

BRASÍLIA-DF, 27 DE FEV DE 2025

UNIVERSIDADE DE BRASÍLIA
FACULDADE DE TECNOLOGIA
DEPARTAMENTO DE ENGENHARIA MECÂNICA
PROGRAMA DE PÓS-GRADUAÇÃO EM CIÊNCIAS MECÂNICAS

EVALUATION OF AMAZONIAN WOOD RESIDUE BLENDS FOR DECENTRALIZED ENERGY RECOVERY: COMBUSTION PARAMETERS AND POTENTIAL EMISSIONS

MAYARA GABI MOREIRA

DISSERTAÇÃO DE MESTRADO SUBMETIDO AO DEPARTAMENTO DE ENGENHARIA MECÂNICA DA FACULDADE DE TECNOLOGIA DA UNIVERSIDADE DE BRASÍLIA, COMO PARTE DOS REQUISITOS NECESSÁRIOS PARA A OBTENÇÃO DO GRAU DE MESTRE EM CIÊNCIAS MECÂNICAS.

APROVADA POR:

Prof. Dr. Edgar Amaral Silveira, ENM/UnB (http://lattes.cnpq.br/3018359232062233)
Orientador

Prof. Dr. José Luiz Francisco Alves, DEER /UFPB (http://lattes.cnpq.br/5701667636756731)
Examinador externo

Prof. Dr. Thiago de Paula Protásio, DCF-ESAL/UFLA (http://lattes.cnpq.br/3847639263484797)
Examinador externo

Prof. Dr. Tiago José Pires de Oliveira, DQM /UFLA (http://lattes.cnpq.br/5244533061705562)
Examinador externo

BRASÍLIA, 27 DE FEV DE 2025

FICHA CATALOGRÁFICA

MOREIRA, MAYARA GABI

Evaluation of amazonian wood residue blends for decentralized energy recovery: combustion parameters and potential emissions

2025, 72 p., 201x297 mm

(PPGCM/FT/UnB, Mestre, Ciências Mecânicas, 2025).

Dissertação de Mestrado – Universidade de Brasília. Faculdade de Tecnologia.

Programa de Pós-Graduação em Ciências Mecânicas

REFERÊNCIA BIBLIOGRÁFICA

MOREIRA, M.G. Evaluation of amazonian wood residue blends for decentralized energy recovery: combustion parameters and potential emissions. Programa de Pós-Graduação em Ciências Mecânicas, Universidade de Brasília – Faculdade de Tecnologia, Brasília, DF, 74p.2025

CESSÃO DE DIREITOS

AUTOR: Mayara Gabi Moreira

TÍTULO: Evaluation of amazonian wood residue blends for decentralized energy recovery: combustion parameters and potential emissions.

GRAU: Mestre ANO: 2025

_____

MAYARA GABI MOREIRA
mayaragabimoreira05@gmail.com

Dedico este trabalho à minha querida família, cujo apoio incondicional tornou esta conquista possível.

AGRADECIMENTOS

Agradeço imensamente ao meu orientador, cujo brilhante direcionamento e apoio inestimável foram fundamentais ao longo desta trajetória. Sou profundamente grata aos meus pais, que me proporcionaram suporte e tempo para me dedicar ao mestrado, e ao meu marido, por seu incentivo constante, mesmo nos momentos de cansaço, sempre acreditando no meu potencial. Também expresso minha gratidão aos meus irmãos e aos colegas do LEA, que tornaram esta jornada mais leve e enriquecedora.

A realização deste trabalho também contou com o apoio financeiro do programa de P&D da ANEEL, por meio do projeto PD-08567-0123/2023, bem como da FAPDF e da CAPES, aos quais expresso minha sincera gratidão pelo suporte concedido.

RESUMO

Os sistemas descentralizados de energia na Amazônia enfrentam desafios significativos, incluindo a dependência de energia baseada em diesel não renovável, elevados custos de transporte e acesso limitado a alternativas sustentáveis. No entanto, a biomassa lenhosa proveniente de práticas de manejo florestal sustentável (MFS) está prontamente disponível na região. Ainda assim, dados abrangentes sobre cinética de combustão, parâmetros termodinâmica e emissões são escassos na literatura. Este estudo investiga o potencial de resíduos de biomassa de seis espécies madeireiras amazônicas—*Peltogyne lecointei* (S1), *Erisma uncinatum* (S2), *Martiodendron elatum* (S3), *Handroanthus incanus* (S4), *Dipteryx odorata* (S5) e *Allantoma decandra* (S6)—provenientes de MFS como recursos energéticos renováveis. Quatro misturas distintas desses resíduos foram avaliadas. Foram empregadas análise termogravimétrica e modelagem cinética isoconversional e DAEM para investigar o comportamento de combustão sob diferentes taxas de aquecimento. A validação dos modelos cinéticos com perfis experimentais e preditos de perda de massa apresentou fortes correlações (erro absoluto médio < 6 %), ressaltando a robustez da metodologia aplicada. Os valores de E_α variaram de 150 a 260 kJ mol $^{-1}$, evidenciando a heterogeneidade das biomassas oriundas de MFS. As análises termodinâmicas revelaram entropia favorável ($\Delta S^{\neq}$ = -78 a 125 J mol $^{-1}$ K $^{-1}$) e energia livre de Gibbs ($\Delta G^{\neq}$ = 170 a 215 kJ mol $^{-1}$), indicando um elevado potencial de recuperação de energia. Os fatores de emissão de CO (2,797–2,905 toneladas MJ $^{-1}$), CO_2 (67,109–69,773 toneladas MJ $^{-1}$), SO_2 (0,043 – 0,056 toneladas MJ $^{-1}$) e NO_X (0,008–0,011 toneladas MJ $^{-1}$) demonstraram uma pegada ambiental reduzida em comparação com combustíveis fósseis. Além disso, os valores de captura de CO_2 (1,677 – 1,776 toneladas por tonelada de biomassa) ressaltam o potencial do sistema bioenergético para mitigação de carbono. Esses achados estão alinhados com os Objetivos de Desenvolvimento Sustentável da ONU (ODS 7: Energia Acessível e Limpa, e ODS 13: Ação Climática), ao viabilizar a hibridização de sistemas dependentes de diesel com energia renovável de biomassa em regiões remotas da Amazônia. Isso proporciona soluções sustentáveis para os desafios de acesso à energia e impulsiona iniciativas de energia limpa. As informações obtidas por meio da modelagem da cinética de combustão são cruciais para aprimorar o design, a otimização e a escalabilidade de sistemas energéticos baseados em biomassa, possibilitando sua integração eficiente em aplicações em larga escala.

Palavras-chave: Eficiência na Combustão de Biomassa; Cinética de Degradação Térmica; Transição Energética Sustentável; Estratégias de Redução de Emissões; Integração de Energias Renováveis.

ABSTRACT

Decentralized energy systems in the Amazon face significant obstacles, including reliance on non-renewable diesel-based energy, elevated transportation costs, and limited access to sustainable alternatives. Nevertheless, woody biomass derived from sustainable forest management (SFM) practices is readily available in the region. However, comprehensive data on combustion kinetics, thermodynamics parameters, and emissions remain scarce in the literature. This study investigates the potential of biomass residues from six Amazonian wood species— *Peltogyne lecointei* (S1), *Erisma uncinatum* (S2), *Martiodendron elatum* (S3), *Handroanthus incanus* (S4), *Dipteryx odorata* (S5), and *Allantoma decandra* (S6)—sourced from SFM as renewable energy resources. Four unique blends of these residues were evaluated. Thermogravimetric analysis and isoconversional and DAEM kinetic modeling were employed to analyze combustion behavior under different heating rates. The validation of kinetic models using experimental and predicted mass loss profiles showed strong correlations (MAPE < 6 %), underscoring the robustness of the applied methodology. The E_α values ranged from 150 to 260 kJ mol $^{-1}$, highlighting the heterogeneity of SFM-derived feedstocks. Thermodynamic analyses revealed favorable entropy ($\Delta S^{\neq}$ = −78 to 125 J mol $^{-1}$ K^{-1}) and Gibbs free energy ($\Delta G^{\neq}$ = 170 to 215 kJ mol $^{-1}$), indicating efficient energy recovery potential. Emission factors for CO (2.797–2.905 tons MJ $^{-1}$), CO_2 (67.109–69.773 tons MJ $^{-1}$), SO_2 (0.043 – 0.056 tons MJ $^{-1}$), and NO_X (0.008–0.011 tons MJ $^{-1}$) showed a reduced environmental footprint compared to fossil fuels. Additionally, CO_2 uptake values of 1.677 – 1776 tons per ton of biomass underscore the bioenergy system's potential for carbon mitigation. These findings align with the United Nations Sustainable Development Goals (SDG 7: Affordable and Clean Energy, and SDG 13: Climate Action) by paving the way for hybridizing diesel-reliant systems with renewable biomass energy in remote Amazonian regions. They provide sustainable solutions to energy access challenges while advancing clean energy initiatives. Insights from combustion kinetics modeling are crucial for enhancing biomass-based energy systems' design, optimization, and scalability, enabling their efficient integration into large-scale applications.

Keywords: Biomass Combustion Efficiency; Thermal Degradation Kinetics; Sustainable Energy Transition; Emission Reduction Strategies; Renewable Energy Integration.

LIST OF FIGURES

LIST OF TABLES

LIST OF ABBREVIATIONS AND ACRONYMS

DAEM – Distributed Activation Energy Model

DTG – Derivative Thermogravimetry

E – Activation Energy

EY – Energy Yield

FC – Fixed Carbon

FWO – Flynn-Wall-Ozawa Method

HPLC – High-Performance Liquid Chromatography

HHV – Higher Heating Value

MC – Moisture Content

MAPE – Mean Absolute Percentage Error

NDVI – Normalized Difference Vegetation Index

OWtE – Organic Waste-to-Energy

RB – Raw Blend

SIN – National Interconnected System

SY – Solid Yield

SFM – Sustainable Forest Management

TGA – Thermogravimetric Analysis

UF – Urban Forests

UFW – Urban Forest Waste

VM – Volatile Matter

LIST OF SYMBOLS

$C_{\%,raw}$ – Carbon content on raw biomass (dry basis)

α – Conversion

β – Heating Rate

$\Delta H^{\neq}$ – Enthalpy Change

$\Delta S^{\neq}$ – Entropy Change

$\Delta G^{\neq}$– Gibbs Free Energy Change

A_{α} – Pre-Exponential Factor

E – Activation Energy

E_{α} – Activation Energy as a Function of Conversion

E_C – Emissions Factor of Carbon Dioxide

E_{CO} – Emissions Factor of Carbon Monoxide

E_{CH_4} – Emissions Factor of Methane

E_{CO_2} – Emissions Factor of Chemically Pure Carbon

E_{NO_X} – Emissions Factor of Nitrogen Oxides

E_{SO_2} – Emissions Factor of Sulfur Oxide

f(α) – Reaction Model Function

h - Planck constant

k – Reaction Rate Constant

k_b – Boltzmann constant

m – Sample Mass

m_0 – Initial Sample Mass

m_f– Final Sample Mass

MM_{CO_2} – molar mass of CO_2

MM_C – molar mass of carbon

R – Universal Gas Constant

T – Temperature

T_P – Peak Temperature

t – Time

ρ – Density

SUMMARY

1. INTRODUCTION

To advance Sustainable Forest Management (SFM) and conservation, Brazil has implemented a system of public forest concessions, designating them as production forests . Governed by the Public Forest Management Law (Law nº 11.284/2006) (BRAZIL, 2006), these concessions allow private companies to manage forests sustainably, restore ecosystems, and utilize forest products and services within national public and private forest conservation units (BRAZIL, 2006; ITTO, 2019). This initiative combines legal timber harvesting with conservation efforts, adhering to strict technical standards and environmental regulations while fostering local socioeconomic growth (SÁ et al., 2024).

Brazil ranks as one of the largest producers and consumers of tropical logs, mainly sourced under sustainable forest management practices in the Amazon basin (BRAZIL, 2006; ITTO, 2023; SFB; IPAM, 2011). In 2022, the production of logs from Amazonian forests amounted to 29.2 million m^3 (ITTO, 2023). However, due to relatively low efficiency in converting these logs into sawn timber, Brazil does not rank among the top five global producers of sawn wood (BRAZIL, 2006; ITTO, 2023).

The mechanical processing efficiency of logs in Brazil, established at 35% under CONAMA Resolution 474/2016, indicates that 6.5 out of every 10 logs processed result in waste. Depending on the quality of the logs, this efficiency may be even lower, raising environmental concerns (LUZ et al., 2021). To address this, the National Solid Waste Policy (Law nº 12.305/2010) promotes the utilization of wood residues to create value-added products, enhancing the sustainability of the wood production chain (BRAZIL, 2010). Biomass residues, especially those derived from SFM, emerge as a promising renewable energy source. However, successful implementation demands a detailed understanding of the combustion, thermokinetic properties, and physicochemical characterization of selected biomass residues, as these characteristics influence energy recovery and emission profiles, being relevant for the design of more efficient reactors in converting woody biomass into bioenergy.

Decentralized energy systems are essential for improving energy access in remote regions like the Amazon (SILVEIRA et al., 2025). The region relies heavily on diesel-based energy, contributing to greenhouse gas (GHG) emissions, high logistical costs, and limited energy security (Sá et al., 2024). These factors highlight the urgent need for sustainable, localized energy solutions that support economic development while preserving the environment.

Integrating biomass-powered thermoelectric systems into existing diesel-based energy networks offers a feasible route to establishing hybrid systems in the Amazon. Such systems, which blend renewable biomass energy with traditional diesel generators, have the potential to significantly reduce GHG emissions and increase energy independence in isolated communities (DE OLIVEIRA et al., 2024). However, successful implementation demands a detailed understanding of selected biomass residues' combustion and thermokinetic properties, as these characteristics influence energy recovery and emission profiles (MORTARI et al., 2018).

Thermogravimetric analysis (TGA) and advanced kinetic modeling are pivotal for assessing biomass combustion performance (BARZEGAR et al., 2020). These techniques elucidate energy release mechanisms, activation energy, and thermal stability, facilitating the optimization of combustion conditions (BARZEGAR et al., 2020). Although various studies have explored biomass as a renewable energy source, critical gaps remain regarding the thermokinetic and environmental properties of residues derived from SFM practices. While these studies have provided important insights into improving industrial applications, significant gaps remain in understanding the thermokinetic properties of these residues for energy recovery. Thus, there is ample opportunity for further research to explore advanced modeling techniques that can optimize the energy recovery processes of SFM residues (LIMA et al., 2020a; PROTÁSIO et al., 2020; SÁ et al., 2024).

A thorough understanding of biofuel combustion is fundamental for effective use in decentralized systems. Non-isothermal methods are widely used in kinetic analyses and are divided into model-free and model-fitting approaches. Model-free techniques are favored for their simplicity, using kinetic plots across multiple heating rates to determine parameters without assuming reaction mechanisms (CAI; WU; LIU, 2012; KIM; EOM, 2006; WHITE; CATALLO; LEGENDRE, 2011). Common model-free methods include Flynn-Wall-Ozawa (FWO) (FLYNN; WALL, 1965), Kissinger-Akahira-Sunose (KAS) (KISSINGER, 1956), Friedman (FRIEDMAN, 1964), Vyazovkin (VYAZOVKIN, 1997), Coats-Redfern(ESPITALIE et al., 1987), e Starink (STARINK, 1996), which calculate activation energy and pre-exponential factors based on temperature and conversion data. These approaches have been applied to materials such as plum and fig pomace, pearl millet, bamboo residues, and other biomass types (BOUBACAR LAOUGÉ; MERDUN, 2020; HU et al., 2019; KATNIĆ et al., 2022). Additionally, thermodynamic parameters – enthalpy ($\Delta H^{\neq}$), entropy ($\Delta S^{\neq}$), and Gibbs free energy ($\Delta G^{\neq}$) – are crucial for understanding thermal process feasibility, energy potential, and system design (MUMBACH et al., 2022).

Model-fitting techniques, such as the Distributed Activation Energy Model (DAEM), complement these methods by offering a multi-reaction framework that accounts for the simultaneous decomposition of biomass components like hemicelluloses, cellulose, and lignin. The three-parallel DAEM approach effectively deconvolutes these reactions by representing variations in bond strengths (CHEN et al., 2015b). Despite its complexity, simplified methodologies like the Miura-Maki and Scott methods (MIURA; MAKI, 1998; SCOTT et al., 2006) have facilitated its application to biomasses such as pine wood, wheat stalks, and sugarcane bagasse (ARENAS; NAVARRO; MARTÍNEZ, 2019; CHEN et al., 2015b).

Despite the growing body of research on the bioenergy potential of lignocellulosic biomass, significant knowledge gaps persist in the thermokinetic analysis and emission factors of Amazonian lignocellulosic residues. Studies on biomass types like açaí seeds, guarana seeds, tucumã endocarp, and Brazil nuts have focused on pyrolysis and combustion kinetics (BARONI et al., 2016; COLPANI et al., 2022; LOPES; PEREIRA; TANNOUS, 2018; LOPES; TANNOUS; RUEDA-ORDÓÑEZ, 2016; SANTOS et al., 2020). However, most research emphasizes kinetic parameter determination, overlooking a more comprehensive evaluation of other pertinent aspects. Consequently, a broader investigation into the thermochemical behavior of Amazonian biomass residues is urgently required.

1.1 Objectives

This study aims to apply experimental techniques (TGA) and numerical models (isoconversional methods and DAEM) to evaluate the combustion behavior and thermodynamic properties of sustainable management residues from the Amazon region, focusing on their application in decentralized energy generation systems.

The specific objectives are:

- Investigate the thermal properties of Amazonian biomass residues at different heating rates using thermogravimetric analysis (TGA).
- Determine the kinetic parameters by applying isoconversional methods (Friedman, Flynn-Wall-Ozawa (FWO), Kissinger-Akahira-Sunose (KAS), and Starink) as well as the Distributed Activation Energy Model (DAEM).
- Estimate the lignocellulosic composition of Amazonian biomass residues using DAEM.

- Evaluate key thermodynamic parameters, including enthalpy ($\Delta H^{\neq}$), entropy ($\Delta S^{\neq}$), and Gibbs free energy ($\Delta G^{\neq}$), to elucidate the fundamental thermal decomposition mechanisms.
- Assess CO_2 uptake and quantify potential gaseous emissions (CO, CO_2, CH_4, SO_2, and NO_X) during the combustion of biomass residues.

This multifaceted approach aims to provide crucial insights into the potential of Amazonian wood residues as a sustainable energy vector. Furthermore, the present work stands out as pioneering in using DAEM to determine kinetic parameters and lignocellulosic composition in Amazonian biomass.

2 STATE OF THE ART

Combustion and pyrolysis are well-established techniques for biomass conversion into bioenergy, and their applications have been extensively studied. Despite this, there is a notable gap in the literature regarding thermokinetic analysis and gas emission factors for lignocellulosic residues specific to the Amazon. This chapter provides a summary of recent research addressing these aspects. Table 1 summarizes studies on experimental and numerical techniques to analyze combustion and pyrolysis of Amazonian biomass.

Baroni et al. (2016) conducted a study aimed at discussing the applicability of isoconversional methods in estimating the activation energy and pre-exponential factor for biomass pyrolysis, specifically the endocarp of tucumã, a native species from the Amazon. TG and DTG experiments were performed with 5, 10, and 20 °C min^{-1} heating rates in a nitrogen inert atmosphere. The isoconversional methods (Flynn - Wall - Ozawa, modified Coats - Redfern, Friedman, and Vyazovkin) were applied to the experimental data. This resulted in average activation energies of 147.25, 144.64, 160.47, and 144.96 kJ mol^{-1}, respectively, and pre-exponential factors ranging from 9.75 to 11.95 log s^{-1}. The simulations showed that the kinetic parameters calculated with the Flynn - Wall - Ozawa and Vyazovkin methods exhibited a fairly satisfactory agreement with the experimental data, with small relative deviations (9.0 and 9.3%, respectively). Consequently, the authors concluded that the use of isoconversional models is attractive because they are easy to apply and generate satisfactory approximations for real kinetic parameters, especially for biomass that shows or resembles a single peak in the DTG (BARONI et al., 2016).

Table 1 - Literature summary of studies concerning thermokinetic analysis and emission factors for lignocellulosic Amazon waste.

Feedstock	Reaction type / Index	Correlation / Methods	Ref.
Guarana seed	Pyrolysis/ Combustion	Kinetic parameters (Vyazovkin method)	(LOPES; PEREIRA; TANNOUS, 2018)
Guarana seed	Pyrolysis/ Combustion	Kinetic parameters (Friedman, FWO, modified Coats-Redfern, and Vyazovkin methods)	(LOPES; TANNOUS; RUEDA-ORDÓÑEZ, 2016)
Piptocoma discolor	Pyrolysis/ Combustion	Kinetic parameters (consecutive reaction method)	(RIVERA et al., 2023)
Tucumã endocarp	Pyrolysis	Kinetic parameters (Friedman, FWO, modified Coats-Redfern, and Vyazovkin)	(BARONI et al., 2016)
Brazil nut	Pyrolysis	Kinetic parameters (Starink, FWO, KAS, and Vyazovkin) Thermodynamics parameters Pyrolysis behavior indexes	(COLPANI et al., 2022)
Açai seed	Pyrolysis	Kinetic parameters (FWO and KAS methods) Thermodynamics parameters	(SANTOS et al., 2020)
Açai seed	Pyrolysis	Kinetic parameters (Friedman, FWO, modified Coats–Redfern, Starink, and Vyazovkin) Yield of pyrolysis products and Identification of bio-oil compounds	(OLIVEIRA et al., 2023)
Peach palm seed	Pyrolysis	Kinetic parameters (FWO, KAS, Starink, and Vyazovkin) Gas emissions	(SANTOS et al., 2022)
Buriti and Inaja seed	Pyrolysis	Kinetic parameters (FWO, KAS, Starink, Tang, and Vyazovkin) Thermodynamics parameters Gas emissions	(SANTOS et al., 2023)

Source: Author.

In 2016, Lopes et al. (2016) analyzed the kinetics of the thermal decomposition of guaraná seed residues using a thermogravimetric analyzer in a synthetic air atmosphere, with heating rates of 5, 10, and 15 °C min^{-1}, from ambient temperature up to 900 °C (LOPES; TANNOUS; RUEDA-ORDÓÑEZ, 2016). The activation energy, reaction model, and pre-exponential factor were determined using four isoconversional methods (Friedman, FWO, modified Coats-Redfern, and Vyazovkin), master plots, and linearization of the conversion rate equation, respectively. A scheme of two progressive reactions was applied, validating the kinetic parameters for first-order reactions and two-dimensional diffusion models for the oxidative pyrolysis (149.57 kJ mol^{-1}, 6.97×10^{10} s^{-1}) and combustion (77.98 kJ mol^{-1}, 98.61 s^{-1}) stages, respectively. The comparison between theoretical and experimental conversion rates showed good agreement, with an average deviation of less than 2%, indicating that these results can be

used for modeling the thermal compilation of guarana seed residues. These results demonstrate the feasibility of using guarana residues in thermal decomposition processes.

Continuing their studies, Lopes et al. (2018) investigated the thermal decomposition kinetics of guarana seed residues in inert and oxidizing atmospheres (LOPES; PEREIRA; TANNOUS, 2018). The experiments were conducted using a thermogravimetric analyzer with heating rates of 5, 10, and 15 °C min^{-1}. To estimate the activation energies, the isoconversional method of Vyazovkin (1997) was used, resulting in values of 52–140 kJ mol^{-1} for the inert atmosphere and 71–171 kJ mol^{-1} for the oxidizing atmosphere (VYAZOVKIN, 1997). Additionally, independent parallel reaction schemes were applied, with three reactions for the inert atmosphere and six for the oxidizing one, enabling accurate modeling of the conversion rates. The modeling showed excellent agreement with the experimental data, with an absolute deviation of less than 4%, confirming the suitability of the models. These results suggest that kinetic models can be applied in developing and optimizing thermochemical processes, such as biomass pyrolysis and combustion, using guarana residues or similar biomass (LOPES; PEREIRA; TANNOUS, 2018).

SANTOS et al., 2020, 2022, 2023 conducted a series of important studies on the pyrolysis of various seeds from the Amazon, including açaí, buriti, inaja, and Peach palm (SANTOS et al., 2020, 2022, 2023). These studies aimed to evaluate the energy potential of these biomasses through thermogravimetric analysis, determining crucial kinetic and thermodynamic parameters for developing biomass conversion processes into bioenergy. Using isoconversional methods and mass spectrometry coupled with thermogravimetry (TG-MS), these studies provided valuable insights into the thermal decomposition characteristics and the gaseous products released during pyrolysis, significantly contributing to the optimization of thermochemical processes for sustainable energy generation in the Amazon region.

Firstly, Santos et al. (2020) investigated açaí seeds (*Euterpe oleracea Mart.*), determining the kinetic and thermodynamic parameters of the pyrolysis process for energy recovery. Thermogravimetric curves were obtained in the 30–900 °C range under an inert atmosphere, with heating rates of 5, 10, 15, and 20 °C min^{-1}. Using the FWO and KAS methods, the activation energy (E_α) and pre-exponent factor (A_α), were determined, with average E_α values of 159.12 kJ mol^{-1} for FWO and 157.62 kJ mol^{-1} for KAS. The thermodynamic parameters of enthalpy ($\Delta H^{\neq}$), entropy ($\Delta S^{\neq}$), and Gibbs free energy ($\Delta G^{\neq}$) were calculated, with a higher heating value of 21.1 MJ kg^{-1} (SANTOS et al., 2020).

Subsequently, Santos et al. (2022) analyzed the pyrolysis of Peach palm seeds (*Bactris gasipaes* (Kunth)), determining the activation energy using the FWO, KAS, Starink, and Vyazovkin methods, as well as thermodynamic parameters, under heating rates of 5, 10, 20, 30, and 40 °C min^{-1}. The average activation energies ranged from 153.22 to 155.00 kJ mol^{-1} according to the isoconversional methods and 153.5 kJ mol^{-1} using the Vyazovkin method. TG- MS analysis identified the gases released during pyrolysis, including H_2O, CO_2, CO, aldehydes, esters, carboxylic acids, and saturated and unsaturated hydrocarbons. Peach palm seeds' proximate analysis and chemical composition were like other lignocellulosic biomasses, with a higher heating value (HHV) of 16.5 MJ kg^{-1}. The reaction model determined by the Criado method confirmed the complexity of the pyrolysis process, traversing various reaction models for $\alpha > 0.5$. Pupunha seeds proved promising for bioenergy production through thermochemical processes (SANTOS et al., 2022).

Later, Santos et al. (2023) evaluated the energy potential of buriti (*Mauritia flexuosa* L. f.) and inajá (*Attalea maripa* Aubl. Mart.) seeds for pyrolysis using thermogravimetric analysis, with heating rates of 5, 10, 15, and 20 °C min^{-1} under an inert atmosphere. The isoconversional methods (FWO, KAS, Starink, Tang, and Vyazovkin) were employed to determine the kinetic parameters. The average activation energies were 146.84–145.36 kJ mol^{-1} for buriti seeds and 115.88–112.38 kJ mol^{-1} for inajá seeds. Thermodynamic analysis revealed positive values for enthalpy ($\Delta H^{\neq}$) and Gibbs free energy ($\Delta G^{\neq}$), and negative entropy values ($\Delta S^{\neq}$), indicating that the pyrolysis process is non-spontaneous. However, the small difference between $\Delta H^{\neq}$ and E_{α} (< 5 kJ mol^{-1}) supports the feasibility of these seeds as bioenergy sources. TG-MS analysis identified key gaseous products released during pyrolysis, such as H_2O, CO_2, CO, aldehydes, esters, carboxylic acids, and saturated and unsaturated hydrocarbons, which can be converted into energy and valuable chemicals. The higher heating values (HHV) of buriti and inaja seeds were estimated at 21.3 and 18.0 MJ $kg^{-1,}$ respectively, comparable to other lignocellulosic biomasses. These results highlight the significant potential of buriti and inajá seeds for bioenergy production through thermochemical processes, positioning them as promising biomass resources from the Amazon region (SANTOS et al., 2023).

A study conducted by Colpani et al. (2022) analyzed the pyrolysis kinetics of Brazil nut shells (BNS) and skins (BNH) (*Bertholletia excelsa*) through thermogravimetric analysis in an inert atmosphere. The FWO, KAS, Starink, and Vyazovkin isoconversional methods were applied to estimate kinetic and thermodynamic parameters. This pioneering study, employing TG/DTG and TG-MS (Mass Spectrometry), allowed the identification of gases released at

different temperature ranges. Heating rates varied between 5 and 40 °C min^{-1}. TG-MS analyses highlighted emissions of gases less harmful to the environment than fossil fuels, with significant reductions in CO and CO_2 peaks at higher temperatures. Emission peaks were predominantly observed in the active pyrolysis range (200–450 °C), associated with the highest mass loss: 40.8–46.09% for BNS and 47.73 – 51.10% for BNH. The average activation energy (E_α) values were 138.51–135.59 kJ mol^{-1} for BNS and 153.92–151.94 kJ mol^{-1} for BNH. High pre-exponential factor values (> 10^8 s^{-1}) indicated reaction complexity, corroborated by the master plot method. The pyrolysis of residues proved to be an endothermic and non-spontaneous process, requiring low external energy (< 5 kJ mol^{-1}) for product generation. Thus, the results confirm the feasibility of Brazil nut residue pyrolysis as an effective technique for converting this biomass into energy (COLPANI et al., 2022).

In a recent study, Rivera et al. (2023) focused on determining the thermogravimetric characteristics and kinetic modeling of the pyrolysis and combustion processes of *Piptocoma discolor* (a native species of the South American Amazon, abundant in secondary forests), contributing to the understanding of its energetic use in the Ecuadorian Amazon region (RIVERA et al., 2023). Thermogravimetric analysis was applied to study the thermal decomposition of *P. discolor* biomass under an inert atmosphere and oxygen presence, with a heating rate of 5 °C min^{-1}, from room temperature to 900 °C. A mechanism comprising three independent parallel reactions corresponding to the three main pseudo-components (hemicelluloses, cellulose, and lignin) was employed to detail the pyrolysis process and an additional stage to model the combustion process, including char oxidation. The model successfully replicated the degradation curves for both pyrolysis and combustion, demonstrating a strong fit between experimental and calculated data, with coefficient of variation values below 5% (3.19% for pyrolysis and 2.97% for combustion). The calculated kinetic parameters (pre-exponential factor, activation energy, and reaction order) for the main pseudocomponents were consistent with those reported in lignocellulosic material pyrolysis and combustion studies. These findings confirm that biomass derived from P. discolor can be utilized as an energy source through thermal conversion processes (RIVERA et al., 2023).

Furthermore, Oliveira et al. (2023) also investigated the pyrolysis kinetics of açaí seeds using thermogravimetric analysis under a nitrogen atmosphere, with heating rates of 2, 5, 10, 15, and 20 °C min^{-1}. The isoconversional methods (Friedman, FWO, modified Coats–Redfern, Starink, and Vyazovkin), along with the master plots method, were employed to determine kinetic parameters. The FWO model exhibited the smallest variation, with an average activation

energy of 165.59 kJ mol $^{-1}$. The global average activation energy was 134.76 kJ mol $^{-1}$, and the Arrhenius pre-exponential factor was 1.11×10^{10} s^{-1}. The composition of the bio-oil produced was identified using gas chromatography coupled with mass spectrometry. The pyrolysis of açaí seeds was characterized by a second-order reaction mechanism, with bio-oil yield maximized at moderate temperatures with high heating rates or high temperatures with low heating rates. The bio-oil composition varied significantly depending on temperature and heating rate, influenced by the biomass's extractives and lignin content, favoring the formation of fatty acids and phenolic compounds. These findings underscore the potential of açaí seeds for bio-oil production through pyrolysis (OLIVEIRA et al., 2023).

From the cited studies, it is observed that the majority focused on pyrolysis and the determination of kinetic parameters exclusively. Notably, all employed isoconversional methods or parallel reaction schemes are employed without applying the Distributed Activation Energy Model (DAEM). Thus, the present work's originality becomes evident by uniquely utilizing the DAEM model to numerically determine combustion behavior and kinetic parameters for blends of Amazonian Forest residues. The application of the DAEM model offers significant advantages, such as its ability to more accurately and comprehensively describe the distribution of activation energies in complex processes, enabling a more detailed and realistic analysis of thermochemical reactions (CHEN et al., 2015b; KRISTANTO et al., 2022).

3 THEORETICAL FRAMEWORK

3.1 Challenges and Opportunities in The Use of Biomass in The Amazon Region

The Amazon region is characterized by many isolated riverside communities that need electricity for 270 municipalities not connected to the National Interconnected System (SIN). In these areas, electricity is generated by 265 thermal plants, 97% of which use diesel or fuel oil (MME, 2023a). The vast territorial dispersion of these communities requires the installation of extensive cables to supply energy, resulting in significant challenges in generation and distribution. Additionally, these populations' low income prevents the passing of various operational costs to tariffs and contributes to increased technical losses, leading to considerable financial losses. Decentralized energy generation is limited due to the high transmission and distribution costs, making accessing essential services such as healthcare, education, and other

public services difficult. Therefore, it is crucial to conduct studies that explore local natural resources for energy generation (FLORES et al., 2018; WELFLE, 2017).

In 2023, Brazil mainly relied on renewable energy sources, such as hydropower (68%), wind (15.0%), biomass (5.3%), and solar (4.2%), which together accounted for 92% of the country's energy generation capacity (MME, 2023a). The biomass available in Brazil, including biomass residues, has great potential to meet the energy demand. In 2022, sugarcane (15.4%) and wood with charcoal (9%) were the main biomasses used for energy production (MME, 2023b). The main sources of wood and charcoal are energy forests of Eucalyptus spp. and residues from sustainable forest management plans in the Amazon (IBÁ, 2023).

In 2018, a study revealed the presence of 70 sources of non-wood native biomass in Amazonian extractive reserves, indicating their potential as renewable sources for bioenergy production and their role in supporting isolated communities (FLORES et al., 2018). ARAUJO et al. (2022) surveyed fruit production and residual biomass in Pará and Amazonas between 2017 and 2019, as shown in Figure 1. According to Figure 1, in many cases, the weight of the residues exceeds that of the usable part. This situation can significantly promote sustainable development in rural areas and less developed regions through energy generation from these residues (ARAUJO et al., 2021).

Studies on wood biomass have shown that one ton of processed wood for sawdust and trimming can generate 2.14 tons of cutting residues (NUMAZAWA et al., 2017). LIMA et al., (2020a) identified that approximately 100,000 tons of these residues are produced annually in a Forest Management Area in Pará. Despite Brazilian regulations encouraging their use, these residues are typically stored in managed areas (LIMA et al., 2020b). The energetic utilization of these residues contributes to the sustainability of forest management and diversification and adds value to derived products, aiding in reducing deforestation in the Amazon. However, the variability of cutting residues due to the diversity of species exploited in a Sustainable Forest Management Plan presents a challenge (LIMA et al., 2020a).

Given the significant challenges and opportunities presented by the Amazon’s biomass potential, using this renewable energy source is essential for the sustainability of Brazil's energy matrix. The region's resource diversity offers a pathway for sustainable development and addresses disparities in energy access for isolated communities. However, the logistical and technological barriers demand innovative solutions and effective public policies. Therefore, further research and practical applications are critical to fully harnessing biomass residues fostering an inclusive and sustainable energy sector in the Amazon.

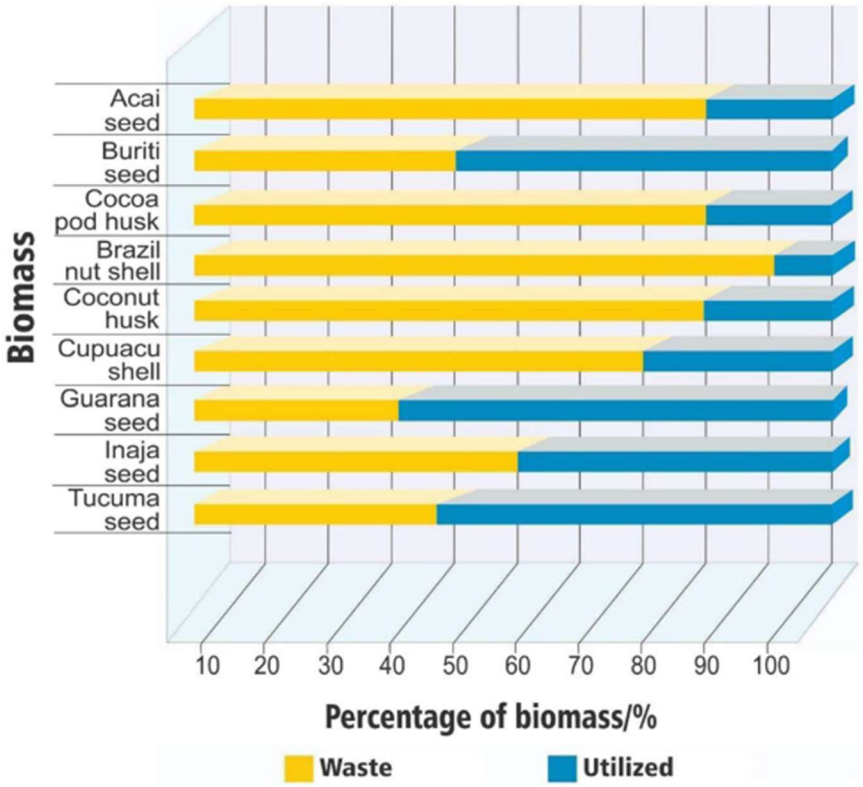

Figure 1 - Percentage of fruits utilized and the amount of waste produced after processing in the states of Amazonas and Pará, Brazil (ARAUJO et al., 2022).

3.2 Biomass: General Characteristics

Biomass, formed from living species such as plants and animals — that is, anything that is now alive or was alive a short time ago, offers significant economic and technical advantages and addresses the growing need for cleaner technologies in response to global warming and climate change (KATNIĆ et al., 2022). In addition to being a sustainable energy source, biomass emits fewer pollutants such as carbon dioxide, sulfur oxides, and nitrogen oxides, playing a key role in reducing fossil fuel consumption in energy production sectors (HEYA et al., 2019).

Common sources of biomass can be categorized into different types (BASU, 2018):

- Agricultural: food grains, ground sugarcane bagasse, corn stalks, straw, seed husks, nut shells, and animal manure.
- Forestry: trees, wood waste, sawdust, and mill scraps.

- Municipal: sewage sludge, fuel derived from waste, food waste, paper waste, and yard clippings.
- Energy Crops: poplars, willows, alfalfa, bluestem prairie, corn, soybeans, canola, and other vegetable oils.
- Biological: animal waste, aquatic species, and biological waste.

Most biomass consists of lignocellulose, the fibrous and non-starchy part of plant materials, primarily composed of cellulose, hemicelluloses, and lignin, as shown in Figure 2. Cellulose is the most prevalent organic compound on Earth and is the main structural component of plant cell walls (BASU, 2018). Cellulose can account for up to 90% (by weight) of cotton and around 33% in other plants. In addition to cellulose, plant cell walls contain hemicelluloses, which has an amorphous, random structure, complementing cellulose's crystalline structure and showing lower hydrolysis resistance. Lignin is a complex phenylpropane polymer crucial in forming plant secondary cell walls. Regarding proportion, lignin accounts for 18% to 25% of the dry weight in hardwood and 25% to 35% in softwood (BASU, 2018).

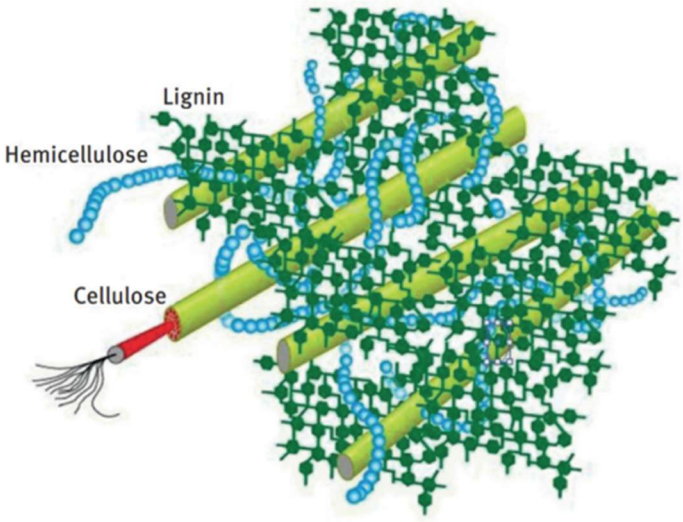

Figure 2 - Representations of the biomass structure and the structures of cellulose, lignin, and hemicelluloses (WANG et al., 2017).

The growing attention given to the cultivation of plants specifically intended for energy generation, known as "energy crops," reflects the importance of biomass in the energy

transition. These crops, predominantly lignocellulosic, usually have short growth cycles, providing high yields and requiring few or no fertilizers, which results in a quick return on investment (BASU, 2018). Additionally, residual biomass, which derives from primary biomass sources such as trees, vegetables, or animals, plays a crucial role. Most biomass waste comes from renewable energy sources, such as food scraps, grass clippings, leaves, and paper. Non-renewable components, such as plastics, glass, and metals, are not classified as biomass, and in some cases, the combustible part of the waste is separated and marketed independently (BASU, 2018).

In summary, biomass is a viable and sustainable solution for producing energy and carbonaceous materials. Its diverse sources and environmental benefits reinforce its essential role in transitioning to a low-carbon economy and mitigating climate change.

3.3 Routes for Biomass Valorization

The main challenges in transitioning from fossil fuels to biomass-based fuels include the large volume, low energy density, and impractical form of untreated solid biomass. To address these limitations, carbonization and torrefaction are employed to produce cleaner and more efficient solid fuels. However, solid biomass faces significant handling, storage, and transportation challenges, highlighting the importance of converting it into liquid or gaseous fuels. These forms offer higher energy density and are easier to store and transport (BASU, 2018).

There are three distinct pathways for biomass conversion. The first, known as the biochemical route, is predominantly used in producing first- and second-generation ethanol. This process involves several stages, such as digestion (anaerobic or aerobic in composting), fermentation, distillation, and hydrolysis, which can be carried out through enzymatic or acidic processes. The second pathway is the physicochemical route, which involves the compression or extraction of vegetable oils for biodiesel production, for example, through the transesterification process.

The third pathway is thermochemical conversion, which involves controlling the heating or oxidation of biomass, as shown in Figure 3 (BASU, 2018; SEO et al., 2022). Thermochemical processes can convert biomass into various products within seconds or minutes, and these products can be enhanced or improved using catalysts or subsequent processes. Thermochemical conversion approaches, including pyrolysis, torrefaction, hydrothermal treatment, gasification, and combustion, have been extensively developed and

applied to valorize biomass into heat, energy, biochar, bio-oil, and syngas. These mature processes have been used to produce heat, energy, and chemicals from coal, oil, and natural gas over the past two centuries (SEO et al., 2022).

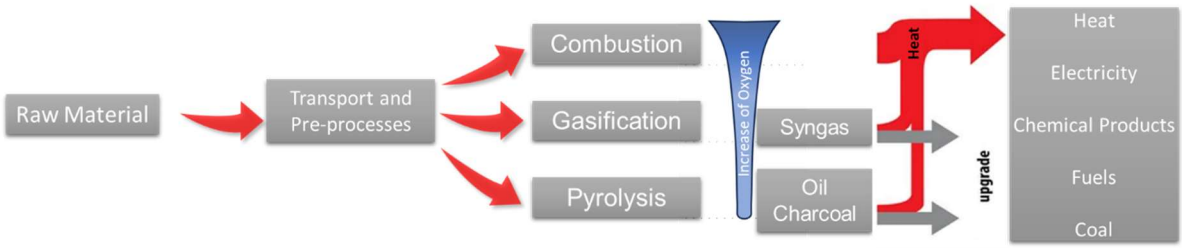

Figure 3 - Thermochemical routes for biomass valorization (Author).

Thermochemical conversion techniques are classified based on the associated oxidation environment, particle size, and heating rate. This classification ranges from applying heat to biomass in oxygen-free environments (endothermic process) to the complete exothermic oxidation of biomass.

Combustion occurs at high temperatures in an oxidative environment, producing heat through the oxidation of biomass rich in carbon and hydrogen, generating CO_2 and H_2O. However, the complex chemical kinetics of reactions during this process can release atmospheric pollutants, such as CH_4, CO, and particulate matter (PM) (SEO et al., 2022). Furthermore, impurities present in the fuel, such as sulfur and nitrogen, are associated with the emission of SO_X and NO_X. Typically, the combustion process is classified based on the type of fuel, which can involve single-fuel combustion or co-combustion of two fuels, and based on the oxygen supply method, such as forced air, pure oxygen, or fuel pretreatment (SEO et al., 2022).

The direct combustion of biomass is one of the primary sources of bioenergy worldwide. Biomass is utilized both as a standalone fuel and as a supplement to fossil fuels in boilers, with the latter option gaining popularity as an efficient and cost-effective way to reduce carbon dioxide emissions from existing fossil fuel power plants. Electricity, essential for all modern economic activities, can be generated by burning biomass to produce steam in boilers, which is then used to drive steam turbines for power generation (BASU, 2018).

Pyrolysis occurs in the complete absence of oxygen. During this process, biomass undergoes thermal decomposition into gas, liquid, and solid fractions, rapidly heated to

temperatures between 300–650 °C (SEO et al., 2022). In pyrolysis, the large molecules present in biomass are broken down into smaller molecules. This process is initiated by heat transfer from the circulating gas to the combustible material, resulting in thermal decomposition. Consequently, various products are generated, including gases such as H_2, CO, CO_2, CH_4, H_2O, and NH_3, as well as hydrocarbon vapors, bio-oil, and charcoal (BASU, 2018).

Gasification is an endothermic process involving the partial oxidation of biomass, where process conditions are adjusted to achieve high yields of gaseous products such as syngas or process gas, containing CO, H_2, CH_4, and CO_2 (SEO et al., 2022). This method converts various types of fuels—fossil-based or not and in solid, liquid, or gaseous forms—into gases with practical applications. For gasification reactions to occur, an appropriate medium is essential, which may include gases, steam, subcritical or supercritical water, and combinations of air and oxygen (BASU, 2018). The resulting gas can be refined and used directly as fuel for engines or upgraded into liquid fuels or chemical feedstocks through biological fermentation or catalytic upgrading processes, including the Fischer-Tropsch process (SEO et al., 2022).

During the torrefaction process, a pretreatment method, biomass undergoes gradual heating to temperatures ranging from 200 °C to 300 °C while being maintained in conditions with minimal or no oxygen exposure. This procedure induces chemical modifications in the structure of the hydrocarbons present in the biomass, resulting in an increased carbon content and a reduced oxygen content. Simultaneously, torrefaction enhances the energy density of the biomass and makes it more prone to moisture absorption. These characteristics add commercial value to wood for energy production and transportation (BASU, 2018).

The valorization of biomass through biochemical, physicochemical, and thermochemical routes offers efficient solutions to overcome challenges associated with using biomass as an energy source, such as energy density and handling. Thermochemical conversion, in particular, stands out for its ability to transform biomass into various valuable products with lower environmental impacts. Combustion, pyrolysis, gasification, and torrefaction are essential to optimize biomass use, promote economic and environmental sustainability, and significantly contribute to the transition to a cleaner energy matrix.

3.4 **Thermogravimetric Analysis**

Thermogravimetry is a thermal analysis technique that monitors changes in the mass of a sample as a function of temperature and/or time. The equipment used, known as a thermobalance, is essential for continuously weighing the sample during the heating or cooling.

Figure 4 shows the thermogravimetric curve (TG) and its derivative concerning time (DTG) for a lignocellulosic biomass sample undergoing combustion. These curves provide two crucial observations: 1) The influence of the decomposition temperature on the type of biomass and 2) The impact of the heating rate on the degradation temperature, specifically the temperature corresponding to the maximum degradation of the main biomass components, DTG_{max}.

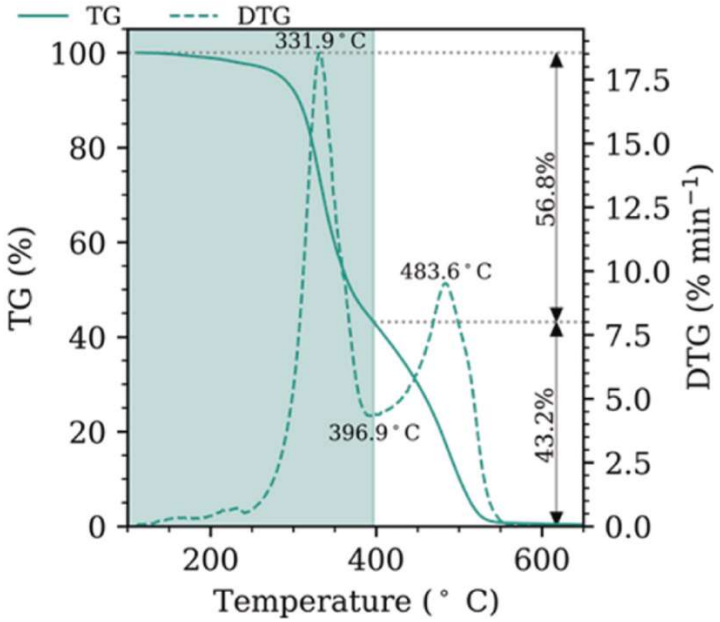

Figure 4 – TGA and DTG curves for the combustion of a lignocellulosic biomass sample (Silveira et al., 2025).

Some biomass species present two main peaks in their DTG curves when air is used as carrier gas. In lignocellulosic biomass, the first peak is predominantly associated with cellulose degradation, and the second mainly with lignin degradation (BRACHI et al., 2015; WILD; WOUTER J. J. HUIJGEN; RICHARD J.A. GOSSELINK, 2014). Moreover, the most established methodology for calculating the activation energy (E_α) from biomass combustion involves performing thermogravimetric analysis (TGA) on the sample, followed by calculations using various methods, such as isoconversional methods. Isoconversional methods, which are independent of the reaction model, require a set of non-isothermal TGA tests to determine the dependence of E_α on the conversion degree (α). The standard for isoconversional kinetic studies is to conduct TGA experiments under multiple non-isothermal conditions, using at least three different heating rates (ALVES et al., 2022d).

12.12 Kinetic Modeling

The kinetics of the combustion reaction of lignocellulosic biomass, as described by the Arrhenius equation, generally follow a heterogeneous conversion process involving solid, volatile, and gas phases (VYAZOVKIN et al., 2011). From Eq. (1), the experimental conversion (α) was calculated.

$$\alpha = \frac{m_i - m}{m_i - m_f} \tag{1}$$

Here m_i is the sample's initial mass (in mg); m is the sample mass at time t (in mg); and m_f is the sample mass (in mg) at 800 °C. The decomposition rate (Eq. (2)) is evaluated by the general expression for biomass combustion kinetics as a function of temperature (T) and conversion (α).

$$\frac{d\alpha}{dt} = k(T) \,.\, f(\alpha) \tag{2}$$

The $(d\alpha/dt)$ can be written as Eq. (3),

$$\frac{d\alpha}{dt} = \beta \frac{d\alpha}{dT} = k(T) \,.\, f(\alpha) \tag{3}$$

where β represents the average heating rate (°C min^{-1}). The $k(T)$ can be defined by Eq. (4),

$$k(T) = A \,.\, e^{\frac{-E_\alpha}{RT}} \tag{4}$$

where E_α (J mol^{-1}) is the apparent activation energy, and A (s^{-1}) is the pre-exponential factor. T (K) is the temperature, and R is the gas constant (8.314 J mol^{-1} K^{-1}). Substituting Eq. (4) into Eq. (3) results in Eq. (5):

$$\frac{d\alpha}{dt} = \beta \frac{d\alpha}{dT} = A \,.\, e^{\frac{-E_\alpha}{RT}} \,.\, f(\alpha) \tag{5}$$

Reorganizing and integrating Eq. (5), the function $g(\alpha)$ is obtained as Eq. (6).

$$g(\alpha) = \int_0^{\alpha} \frac{d\alpha}{f(\alpha)} = \frac{A}{\beta} \int_{T_0}^{T} e^{\frac{-E_\alpha}{RT}} dT \quad (6)$$

3.5.1 Isoconversional Methods

Isoconversional methods are reaction model-independent and require a set of non-isothermal TGA tests to determine the dependence of activation energy on the degree of conversion (ALVES et al., 2022d). The mathematical equations of the main isoconversional methods are presented in Table 2. These methods allow the estimation of activation energy at different conversion levels, thereby eliminating the uncertainty of assuming a specific reaction model. As Vyazovkin et al. (2011) recommended, the conversion range employed to determine the variation in activation energy spans from 10% to 90% (VYAZOVKIN et al., 2011).

Because the isoconversional method can provide a very broad range of values in a small conversion range, making it challenging to interpret these values physically, it is not a reliable way to determine the value of A_α using it (SAHA et al., 2021). Consequently, the ASTM E698 – 18 standard method (Eq. (7)), based on the Kissinger equation, is employed.

$$A_\alpha = \frac{\beta E_{\alpha,i} e^{\left(\frac{E_{\alpha,i}}{R.T_{m,i}}\right)}}{RT_{m,i}^2} \quad (7)$$

Here, $T_{m,i}$ is the temperature determined by the derivative curve (DTG) for each value of β to correlate to the maximum mass loss in the TG curve.

Table 2 – Isoconversional methods formulation.

Method	Formulation	Eq.	Ref.
KAS	$\ln\left(\frac{\beta_i}{T_{\alpha,i}^2}\right) = ln \ln\left(\frac{A_\alpha R}{g(\alpha)E_\alpha}\right) - \left(\frac{E_\alpha}{RT_{\alpha,i}}\right)$	8	(KISSINGER, 1956)
FWO	$\ln(\beta_i) = ln \ln\left(\frac{A_\alpha E_\alpha}{g(\alpha)R}\right) - 5{,}331 - 1{,}052\left(\frac{E_\alpha}{RT_{\alpha,i}}\right)$	9	(FLYNN; WALL, 1965; OZAWA, 1965)
Starink	$\ln\left(\frac{\beta_i}{T_{\alpha,i}^{1,92}}\right) = ln \ln\left(\frac{A_\alpha R^{1,92}}{g(\alpha)E_\alpha^{0,92}}\right) - 0{,}312 - 1{,}0008\left(\frac{E_\alpha}{RT_{\alpha,i}}\right)$	10	(STARINK, 1996)
Friedman	$\ln\left[\beta_i\left(\frac{d\alpha}{dt}\right)_{\alpha,i}\right] = ln \ln[A_\alpha . f(\alpha)] - \left(\frac{E_\alpha}{RT_{\alpha,i}}\right)$	11	(FRIEDMAN, 1964)

β_i is the heating rate.

3.5.2 Distributed Activation Energy Model (DAEM)

The Distributed Activation Energy Model (DAEM) has proven effective in explaining the thermal degradation process of various solid materials, as highlighted in the studies by Cai et al. (2014) and Hu et al. (2016) (CAI; WU; LIU, 2014; HU et al., 2016). This method assumes that degradation involves a series of parallel, irreversible first-order reactions occurring in both inert and oxidative atmospheres.

In the DAEM method with three parallel reactions, three pseudocomponents are introduced to represent hemicelluloses, cellulose, and lignin. The sample mass of the biomass is calculated using Equations (12-14),

$$w = w_1 + w_2 + w_3 \tag{12}$$

$$w_i = x_i\, w \tag{13}$$

$$\sum_{i=1}^{n} x_i = 1 \tag{14}$$

Where w represents the biomass sample mass and x_i denotes the mass fraction corresponding to each component of biomass . When integrated over all activation energies for the reaction of each component in biomass combustion, Equation (5) takes the form of Equation (15).

$$\alpha = \sum_{i=1}^{n} x_i \left(1 - \int_0^{\infty} \exp\left(-\frac{A_i}{\beta}\int_{T_0}^{T} \exp\left(-\frac{E_i}{RT}\,dT\right) f(E)\,dE\right)\right. \tag{15}$$

E, A, β, T and R represent, respectively, the activation energy, the pre-exponential factor, the heating rate, the absolute temperature, and the universal gas constant. The function $f(E)$ indicates the distribution of activation energy, which is modeled by a normal distribution function as described in Equation (16), where σ is the standard deviation of the distribution function, and E_0 is the mean activation energy (LIU et al., 2019). Thus, in the DAEM method for three parallel reactions, 12 distinct variables are considered: the mean and standard deviation of the activation energy, the pre-exponential factor, and the mass fractions attributed to cellulose, hemicelluloses, and lignin.

$$f(E) = \frac{1}{\sigma\sqrt{2\pi}} e^{\left[-\frac{(E-E_0)^2}{2\sigma^2}\right]} \quad (16)$$

Due to the complexity of Equation 15, Miura-Maki (1998) introduced several simplifications to derive Equation 17 (MIURA; MAKI, 1998). Miura-Maki (1998) postulated that each reaction is uniquely defined by its activation energy and employed a “step function” approximation to estimate the proportion at which each reaction occurs.

$$\mathrm{Ln}\left(\frac{\beta_i}{T_{\alpha,i}^2}\right) = \ln\left(\frac{A_\alpha R}{E_\alpha}\right) + 0.6075 - \left(\frac{E_\alpha}{RT_{\alpha,i}}\right) \quad (17)$$

On the other hand, an algorithm developed by Scott et al. (2006) does not require each reaction to be exclusively defined by its activation energy, nor does it use the step function approximation (SCOTT et al., 2006). Equation 18 was employed by Scott to determine the activation energy. This equation effectively calculates the activation energy for a solid composed of multiple components, provided that a single reaction governs the total mass loss in the desired conversion (SCOTT et al., 2006).

$$\begin{aligned}&\frac{1}{\beta_1}\left[T_0 \exp\left(-\frac{E_i}{RT_0}\right) - \frac{E_i}{R}\int_{\frac{E}{RT_0}}^{\infty}\frac{\exp(-u)}{u}du \;- T_1 \exp\left(-\frac{E_i}{RT_1}\right) + \right.\\ &\left.\frac{E_i}{R}\int_{\frac{E}{RT_1}}^{\infty}\frac{\exp(-u)}{u}du\right] = \frac{1}{\beta_2}\left[T_0 \exp\left(-\frac{E_i}{RT_0}\right) - \frac{E_i}{R}\int_{\frac{E}{RT_0}}^{\infty}\frac{\exp(-u)}{u}du \;-\right.\\ &\left.T_2 \exp\left(-\frac{E_i}{RT_2}\right) + \frac{E_i}{R}\int_{\frac{E}{RT_2}}^{\infty}\frac{\exp(-u)}{u}du\right]\end{aligned} \quad (18)$$

4 MATERIALS AND METHODS

4.1 Feedstock

Figure 5 presents the structure of the current study. The feedstock was sourced from a forest concession within the Jacundá National Forest in Rondônia. This national forest, covering 220,644 hectares, is positioned in the northern region of Rondônia, between the municipalities of Porto Velho and Candeias do Jamari. Established in December 2004, it has 112,000 hectares designated for management under the 2009 Annual Forest Concession Plan

(MMAMC, 2025). To highlight the forest, a normalized difference vegetation index (NDVI) analysis was performed on an image of Jacundá Forest (Fig. 5(a)) from CBERS-4A for the year 2022. The cloud-free image was retrieved from the National Institute for Space Research's website (http://www2.dgi.inpe.br/).

According to prior research (SÁ et al., 2024), the feedstock comprises six types of wood residues: *Peltogyne lecointei* (S1), *Erisma uncinatum* (S2), *Martiodendron elatum* (S3), *Handroanthus incanus* (S4), *Dipteryx odorata* (S5), and *Allantoma decandra* (S6), along with four unique blends of these residues. The blends are defined as follows: B1 (S5 and S6), B2 (all species), B3 (S1, S3, S4, and S5), and B4 (S2 and S6) (SÁ et al., 2024). The proportions of each species are outlined in Fig. 5(b). These blends were designed to assess their potential for energy applications, including pelletization, which enhances bioenergy density, simplifies transportation, and improves combustion efficiency for decentralized systems.

The blends were formulated based on ash content and compliance with ISO 17225-2 standards, with B3 and B4 aligning with the requirements for A1 (≤0.7%) and A2 (≤1.2%) quality class pellets. This ensures superior combustion performance and minimizes issues associated with ash. The selection of wood species and their combinations focused on enhancing bioenergy characteristics, such as low ash content, high calorific value, and durability. Additionally, these blends represent practical waste management strategies in Amazonian sawmills. For example, B2 reflects mixed waste streams, while B1 and B4 emphasize species selection based on exploitation intensity and ash content.

4.2 CHEMICAL CHARACTERIZATION

Table 3 outlines the properties of the four blends, while the characteristics of each species are available in prior research (SÁ et al., 2024). The raw wood waste, primarily consisting of rafters, was converted into wood chips and subsequently ground using a Willey knife mill (MICRO MILL R-TE-648, Tecnal © – Brazil). The material was sieved using a mechanical shaker to sort particles according to the size specifications of each standard. Subsequently, the individual species were combined as outlined in Fig. 5(d), oven-dried at 105±2 °C (SL-100/1080I, Solab© – Brazil), and sealed in plastic bags for further analysis.

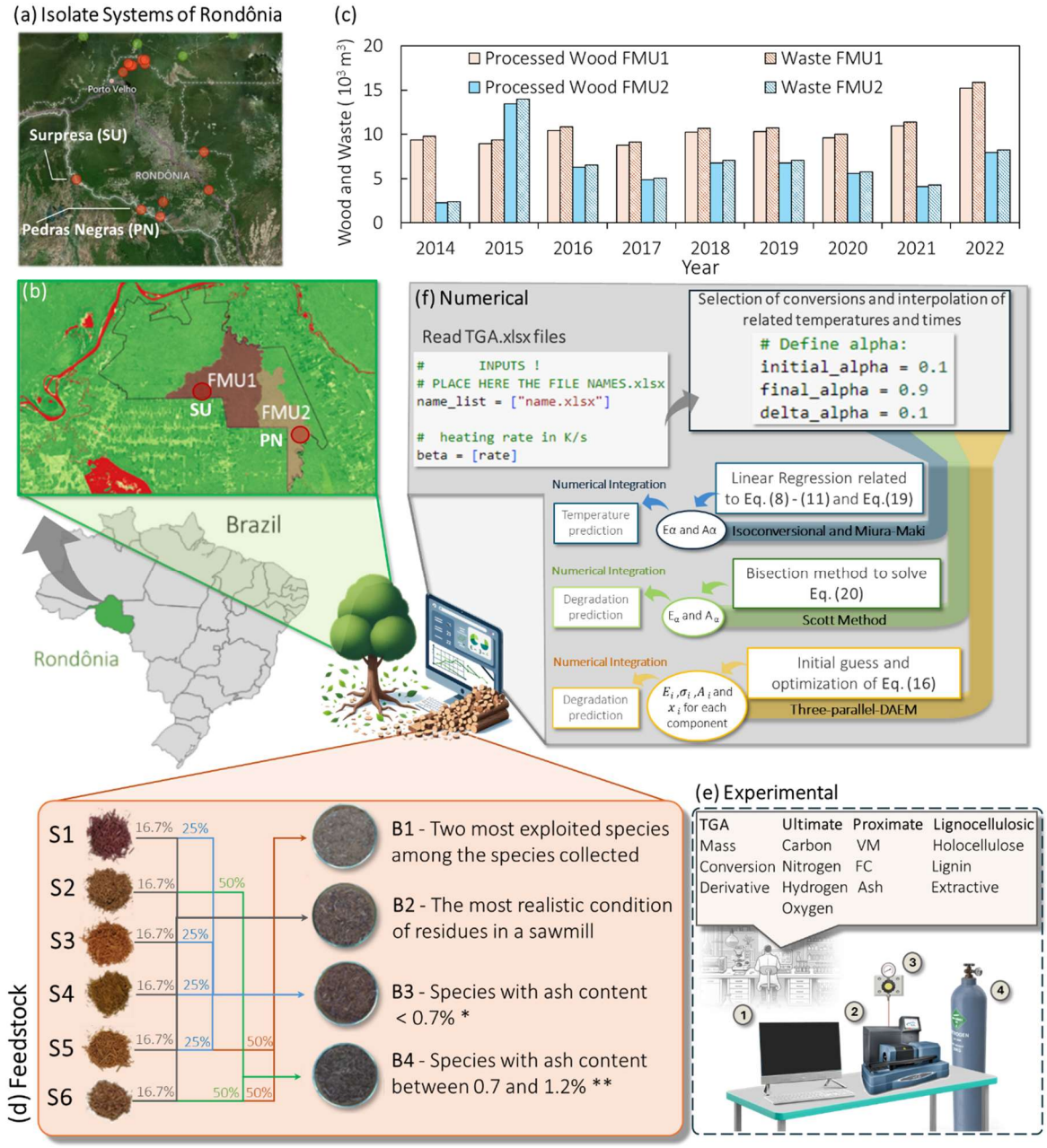

Figure 5 – (a) Isolate Rondônia systems within the forest management units (FMU). (b) Map of Brazil highlighting the Jacundá National Forest by Normalized Difference Vegetation Index (details in green – or positive NDVI values – refer to forest areas) within Rondônia state. (c) Processed wood (51%) and derived waste from processing (49%) of wood logging (EPE, 2018) . (d) Criteria for preparing the wood residue blends. * Limit required for A1 quality class pellets according to ISO 17225-2. ** acceptable range for A2 quality class pellets, according to ISO 17225-2. € Experimental system. 1) Equipment control and data acquiring system (OMNIC© and Qseries© Software). 2) Thermo scientific TGA equipment, 3) Gas control rotameter, 4) N_2 cylinder. (f) Flow chart of the computational procedure (Author).

Each wood species was analyzed for moisture content (ISO 18134-1), ash content, and volatile matter (VM) (ISO 18122 and ISO 18123). Fixed carbon (FC) was calculated by subtracting the volatile matter and ash content from 100% (FC = 100 – VM – ash), and the fuel ratio was determined as FR = FC VM^{-1}. All calculations were dry-based.

Table 3 - Proximate (moisture content (MC), ash content, volatile matter (VM), fixed carbon (FC), and fuel ratio (FR)), ultimate (CHONS, Chlorine, and Heavy Metals in %), calorific (HHV) in MJ kg^{-1}), and bulk density (kg m^{-3}) analysis of obtained blends (adapted from SÁ et al., 2024).

	B1	**B2**	**B3**	**B4**
Lignocellulosic				
Extractives	5.96±0.82	6.98±1.06	9.06±0.98	2.81±1.22
Lignin total	32.09±2.62	32.90±2.06	32.82±1.82	33.07±2.54
Insoluble acid lignin	29.92±2.59	30.72±2.03	30.69±1.79	30.80±2.51
Soluble acid lignin	2.17±0.45	2.18±0.31	2.13±0.26	2.27±0.41
Holocellulose	61.42±2.75	60.51±2.32	57.87±2.07	63.29±2.82
Proximate (%) [a]				
MC	9.88±0.02	10.10±0.06	9.62±0.01	10.98±0.01
ASH	0.53±0.03	0.42±0.01	0.22±0.00	0.83±0.02
VM	84.64±0.11	82.60±0.19	82.69±0.02	82.19±0.04
FC	14.83±0.08	16.98±0.07	17.09±0.01	16.98±0.03
FR	0.18±0.00	0.21±0.00	0.21±0.00	0.21±0.00
Elemental (%) [a, b]				
C	47.15±0.0	47.53±0.1	48.43±0.1	45.74±0.0
H	7.48±0.0	7.46±0.0	7.44±0.0	7.49±0.0
N	0.25±0.0	0.28±0.0	0.27±0.0	0.29±0.1
O[a]	44.53±0.0	44.21±0.1	43.54±0.1	45.55±0.0
S	0.09±0.0	0.10±0.0	0.09±0.0	0.11±0.0
Cl	0.06±0.1	0.05±0.1	0.05±0.1	0.05±0.1
H/C ratio	1.91	1.88	1.84	1.96
O/C ratio	0.71	0.70	0.68	0.75
Calorific (MJ kg^{-1}) [a]				
HHV	20.39±0.1	20.22±0.0	20.77±0.1	20.15±0.1

[a] Data from SÁ et al., 2024. [b] Heavy metals were not identified (< 2ppm).

The ultimate analysis (CHNS) was performed with a PerkinElmer analyzer, adhering to ASTM E777/2008 and E778/2008 standards. The oxygen (content was calculated using the formula O = 100 – C – H – N – S – ash. All calculations were dry-based.

X-ray fluorescence (XRF) measurements for others elements were obtained using energy-dispersive X-ray (EDX) equipment (model 720, Shimadzu) with a rhodium X-ray source tube. XRF spectra were collected under vacuum conditions using two channels (Ti–U and Na–Sc) set at 50 and 15 kV, respectively. Heavy metals were not identified (< 2 ppm) in samples. Calorific value was measured following ISO 18125 with a PARR 6400 bomb calorimeter.

The extractive content was determined by Soxhlet extraction with an ethanol:toluene solvent mixture (1:2 v/v). The contents of insoluble and soluble acid lignin and ash (from extractive-free material) were determined after extraction. The holocellulose content was calculated by subtracting the values of extractives, lignin, and ash from the initial sample mass.

4.3 Thermogravimetric Analysis

The experimental apparatus system is depicted in Fig. 5(e). Combustion tests were conducted in triplicate usina an SDT Q600 TGA from TA Instruments, controlling a relative error below 2%. Dried samples (24h) of 3±0.1 mg with 60 mesh (≤ 250 μm to avoid heat and mass transfer limitations) were heated at a rate of 20 °C min^{-1} from room temperature (~25 °C) to 105 °C. The samples were held isothermally at 105 °C for 20 min to ensure a dry basis. This dehydration stage was excluded from the TG data analysis following the recommendations of (CAI et al., 2018; DA ROCHA et al., 2024). Subsequently, the samples were heated to 800 °C at 20, 30, and 40 °C min^{-1} following previous literature (HU et al., 2024). Combustion was carried out in a synthetic air atmosphere (20% O_2 and 80% N_2) with a flow rate of 100 mL min^{-1} (BARBOSA et al., 2024; CHEN et al., 2020).

The data was processed using the nonparametric Savitzky-Golay smoothing method to minimize data noise, which was applied to refine the derivative conversion curves of combustion, following the recommendations of (CAI et al., 2018; WU et al., 2015).

4.4 Thermokinetic Analytical Methods

4.4.1 Isoconversional Methods

The present study employed the isoconversional methods KAS, FWO, FRIEDMAN, and STARINK, as shown in Table 2. Vectors were created for each isoconversional method to linearize the corresponding equations. For instance, in the Kissinger-Akahira-Sunose (KAS) method, vectors were generated for $\ln\left(\frac{\beta_i}{T_{\alpha,i}^2}\right)$ and $-\left(\frac{1}{RT_{\alpha,i}}\right)$, where β_i represents the heating rate and $T_{\alpha,i}$ is the temperature at a specific conversion for each α. These vectors were used to create

scatter plots and linear regression was performed to determine E_α (activation energy) for each α. The methods were implemented using a numerical routine in *Python 3*, validated in a previous study (MOREIRA; RODRIGUES; SILVEIRA, 2023).

4.4.2 Distributed Activation Energy Model (DAEM)

The present study employs the three main DAEM methods: the complex model with three parallel reactions and the simplified versions by Miura-Maki and Scott. The methods were implemented through a numerical routine in *Python 3*, validated in a previous study (MOREIRA; RODRIGUES; SILVEIRA, 2024).

A nonlinear optimization approach was used to improve the model fit in the method with three parallel reactions. Within this optimization framework, the control variables included activation energies, standard deviations of the Probability Density Functions (PDFs), the pre-exponential factor, and the mass fraction of the three pseudo-components. These parameters were determined through a curve-fitting process using the *curve_fit* function from the *scipy* library in *Python*. The integration limit for dE was assumed to range from 0 to $E_i + 100\sigma_i$ to address the improper integral in Eq. (15). This adjustment considered the simplification of the 4th-degree rational approximate expression for the temperature integral, Eq. (19), and the boundary conditions specified in Table 4 (SENUM; YANG, 1977).

Table 3 - Boundary conditions applied to DAEM.

E_i (kJ mol $^{-1}$)	σ_i (kJ mol $^{-1}$)	A_i (s^{-1})	x_i
0 - infinite	0 - 25	0 - infinite	0 - 1

$$\int_{T_0}^{T} \exp\left(-\frac{E}{RT}\right) dT = \frac{E}{R}\frac{\exp(-x)}{x}\pi(x) \tag{19}$$

where $x = \frac{E}{RT}$ e

$$\pi(x) = \frac{x^3 + 18x^2 + 88x + 96}{x^4 + 20x^3 + 120x^2 + 240x + 120} \tag{20}$$

The accuracy of this fit can be evaluated by calculating the Mean Absolute Percentage Error (MAPE), as described in Equation (21):

$$MAPE = \frac{100}{n}\sum_{i=1}^{n}\left|\frac{Y_i - \hat{Y}_i}{Y_i}\right| \quad (21)$$

where n is the total number of observations, Y_i is the observed value, and $\hat{Y}_i$ is the value predicted by the model.

Similarly to isoconversional methods, the activation energy for the Miura-Maki method was obtained from the slope of a linear regression, and the pre-exponential factor was calculated using Equation (7). On the other hand, the Scott method employs Equation (18). This nonlinear equation can be solved to determine the unknown value of . Upon examination, it is evident that the equation depends exclusively on the activation energy as a variable. The equation can be reformulated as a root-finding problem by grouping all terms on the left-hand side. In this context, the bisection numerical method was chosen to implement the Scott method.

4.4.3 Validation of Kinetic Parameters

This study utilizes four isoconversional methods and three Distributed Activation Energy Model (DAEM) approaches to evaluate the kinetic parameters of biomass blends. The analysis is based on thermogravimetric experiments conducted at heating rates of 20, 30, and 40 °C min $^{-1}$. The methods were applied to predict thermogravimetric curves at 25, 35, and 50 °C min^{-1} heating rates, validating the results and evaluating their predictive accuracy in describing biomass combustion mass decomposition. The predictive capability of kinetic methods plays a critical role in optimizing biomass combustion processes, as it facilitates the simulation of thermal degradation across various operating conditions.

4.4.4 Thermodynamic Parameters

Detailed energy calculations are essential for a thermochemical conversion process to be implemented on an industrial scale. These calculations include evaluating thermodynamic parameters of activated complex such as Gibbs free energy variation ($\Delta G^{\neq}$), enthalpy ($\Delta H^{\neq}$) and entropy ($\Delta S^{\neq}$). These properties are crucial for understanding the feasibility and efficiency of the process at a large scale.

Equations (22–24), derived from transition state theory, are applied to the kinetic parameters of the process to predict these properties. Transition state theory is an approach that describes the formation of a transition state or activated complex during a chemical reaction. This theory enables the correlation between reaction kinetics and changes in thermodynamic properties (SANTOS et al., 2020).

$$\Delta G^{\neq} = E_{\alpha} + RT_m ln\left(\frac{k_b T_m}{hA}\right) \quad (22)$$

$$\Delta H^{\neq} = E_{\alpha} - RT \quad (23)$$

$$\Delta S^{\neq} = \frac{\Delta H^{\neq} - \Delta G^{\neq}}{T_m} \quad (24)$$

Where k_b (1.381 E–23 J K^{-1}) and h (6.626 E–34 J s^{-1}) are the Boltzmann and Planck constants, respectively.

4.5 CO_2 Uptake and Potential Emissions

The CO_2 uptake was calculated based on the carbon content within the blend using the formula presented in Eq. (25):

$$CO_2 uptake \text{ (kg)} = Biomass \times C_{\%,\,raw} \times {MM_{CO_2}}/{MM_C} \quad (25)$$

Where $Biomass$ is the quantity of raw biomass (kg), $C_{\%,\,raw}$ stands for the carbon content on raw biomass (dry basis), MM_{CO_2} the molar mass of CO_2 (44.01 g mol^{-1}) and MM_C the molar mass of carbon, 12.01 g mol^{-1}.

Determining emission factors provides crucial preliminary insights into the potential application of biomass for bioenergy. Furthermore, by leveraging emission factors, functional correlations can be established to predict gaseous emissions, including CO, CO_2, CH_4, SO_2, and NO_X (ALVES et al., 2020b, 2022c; MAJ, 2018a; MAJ et al., 2019). The estimation of emission levels was conducted using ultimate analysis data to evaluate the emissions associated with the combustion of B1, B2, B3, and B4.

Equations (26–31) were applied to calculate the emissions factors (in kg kg^{-1}) of chemically pure carbon (E_C), carbon monoxide (E_{CO}), methane (E_{CH_4}), carbon dioxide (E_{CO_2}),

sulfur oxide (E_{SO_2}) and nitrogen oxides (E_{NO_X}) (ALVES et al., 2020b, 2022c; MAJ, 2018a; MAJ et al., 2019).

$$E_C = C \times u_C \tag{26}$$

$$E_{CO} = \frac{MM_{CO}}{MM_C} \times E_C \times C_{CO/C} \tag{27}$$

$$E_{CH_4} = \frac{MM_{CH_4}}{MM_C} \times E_C \times C_{CH_4/C} \tag{28}$$

$$E_{CO_2} = \frac{MM_{CO_2}}{MM_C} \times \left(E_C - \frac{MM_C}{MM_{CO}} \times E_{CO} - \frac{MM_C}{MM_{CH_4}} \times E_{CH_4} - \frac{26.4}{31.4} \times E_{NMVOC} \right) \tag{29}$$

$$E_{NO_x} = \frac{MM_{NO_2}}{MM_N} \times E_C \times \frac{N}{C} \times N_{NO_x/N} \tag{30}$$

$$E_{SO_2} = \frac{MM_{SO_2}}{MM_S} \times \frac{S}{100} \tag{31}$$

Carbon and nitrogen contents are derived from the biomass ultimate analysis (Table 3). Molar masses (g mol $^{-1}$) for C, CO, CH_4, CO_2, SO_2, and NO_2 are represented by as MM_C, MM_{CO}, MM_{CH4}, MM_{CO_2}, MM_{SO_2}, and MM_{NO_2}, respectively. The fraction of oxidized carbon during combustion is u_C = 0.88. Fractions of carbon released as CO and CH_4 are $C_{CO/C}$ = 0.06 and $C_{CH_4/C}$ = 0.005, respectively. The proportion of nitrogen released as NO_X during the burning of biomass is $C_{NO_x/C}$ = 0.122, and the part of nitrogen emitted as NO_X is $N_{NO_x/N}$ =0.122. The non-methane VOC emission factor is E_{NMVOC} = 0.009. For sulfur dioxide (E_{SO_2}), the sulfur retention in ash was neglected (ALVES et al., 2020b, 2022c; MAJ, 2018a; MAJ et al., 2019). The ratio MM_{SO_2}/MM_S corresponds to the molar mass of sulfur dioxide to sulfur, and *S* denotes the sulfur mass fraction in biomass (Table 3).

5 RESULTS AND DISCUSSION

5.1 Experimental Thermogravimetric Analysis

Figures 6 and 7 illustrate the TG/DTG profiles, 2D combustion conversion contours, and biomass blends' first and second derivative curves. These graphical representations reveal the influence of temperature and heating rates on the decomposition patterns of each sample.

The blend decomposition proceeds through a well-defined sequence of stages, starting with the decomposition of hemicelluloses, cellulose, and lignin (BRACHI et al., 2015; WILD; WOUTER J. J. HUIJGEN; RICHARD J.A. GOSSELINK, 2014). Each stage exhibits unique thermal behaviors and temperature ranges, essential for optimizing biomass utilization in bioenergy applications. The initial stage, moisture release, is evident in the TG curves at temperatures below 200 °C, where all samples behave similarly due to moisture evaporation and the release of low-boiling-point volatile compounds.

Hemicelluloses decomposition generally occurs between 200–300 °C (stage II). Hemicelluloses are characterized by their lower thermal stability compared to cellulose and lignin, contributing to their earlier degradation (MILOS RADOJEVIĆ et al., 2018). The hemicelluloses decomposition is depicted in Figs. 6 and 7 by analyzing the small shoulder before the pronounced peak and in the second derivative curves as the first slight peak. As expected, higher heating rates resulted in intensive α and pronounced peaks with a shift to higher temperatures.

The subsequent decomposition of cellulose occurs at higher temperatures, typically from 240 to 350 °C. Being more thermally stable than hemicelluloses , cellulose requires elevated temperatures to experience significant mass loss (SONG et al., 2019). The cellulose decomposition is attributed to the first peaks of the first DTGs, which were reported between 336–354 °C, 342–360 °C, 338–356 °C, and 333–351 °C and attempted conversion up to 0.55 in this stage for B1, B2, B3 and B4, respectively, depending on the heating rate.

Lignin decomposition occurs over a broader temperature range of 250–500 °C, with a percentage of mass loss of about 40%, reflecting its complex molecular structure, which includes abundant aromatic rings and cross-linked properties that make it more resistant to thermal decomposition (MILOS RADOJEVIĆ et al., 2018; SONG et al., 2019). The decomposition of the lignin can be visualized by the second peaks of the first DTGs between 477–491, 460–474, 446–460, and 481–495 °C for B1, B2, B3 and B4, respectively, depending on the heating rate. Most thermal volatilization events in the blend samples occurred between 200–400 °C, contributing to approximately 60% of the total mass loss. Beyond this range, only 0.5% of mass is lost between 600 and 800 °C, with the remaining ash material.

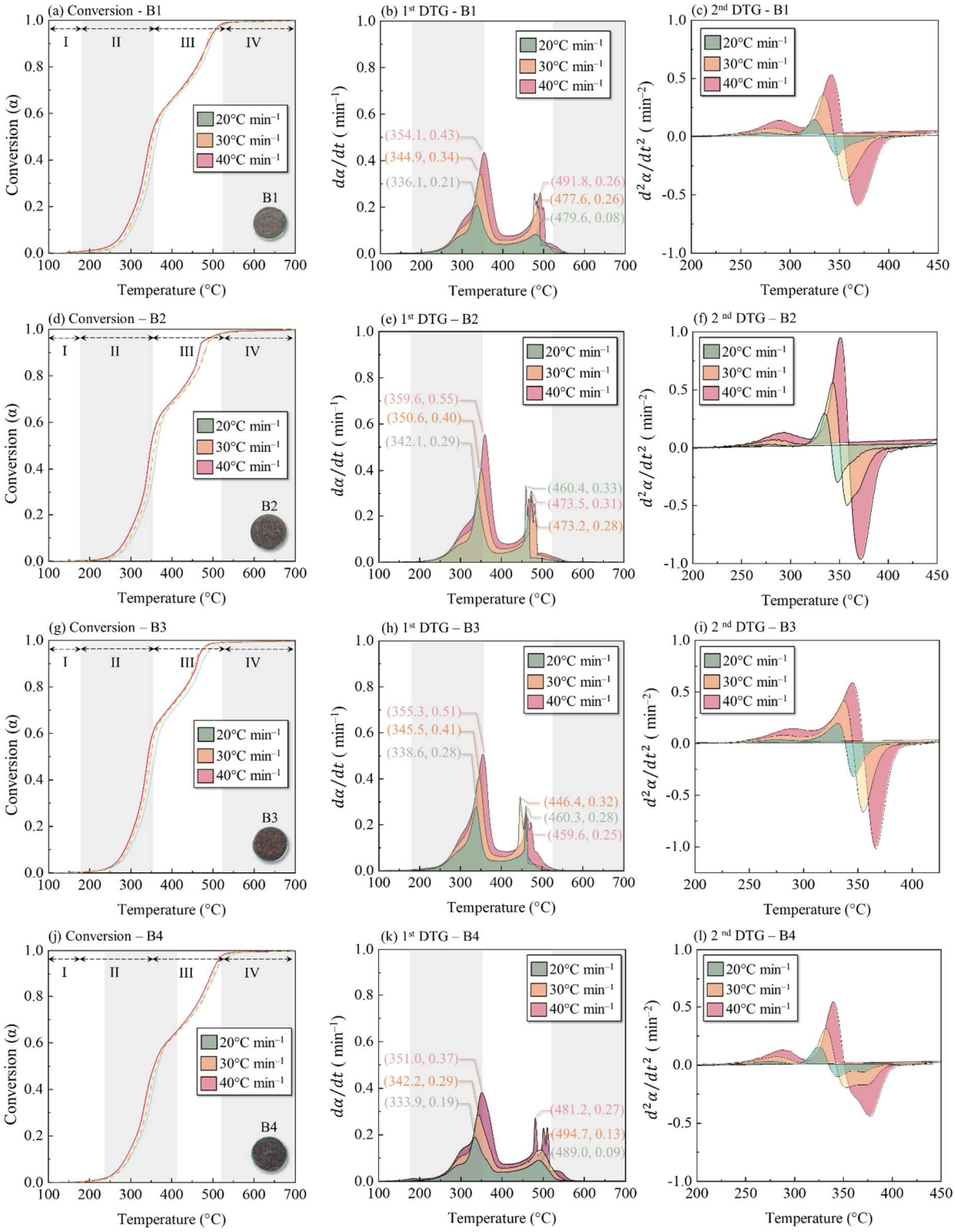

Figure 6 - Conversion curve profiles (α) (a–d), first derivative thermogravimetric (DTG) curves (e–h), and second derivative thermogravimetric (DTG) curves (i–l) associated with blends B1, B2, B3, and B4, respectively.

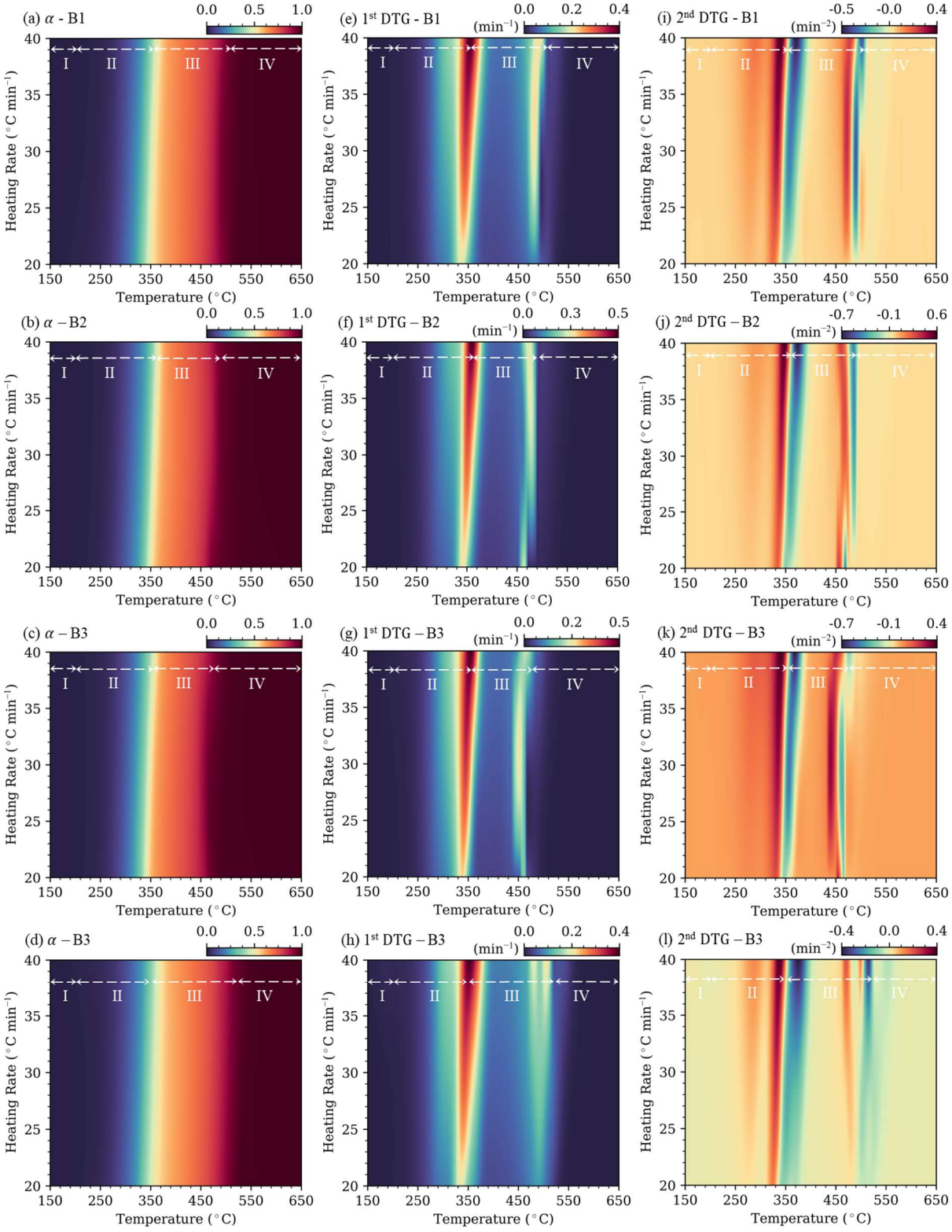

Figure 7 - 2D contour maps for conversion (α) (a–d), first derivative thermogravimetric (DTG) curves (e–h), and second derivative thermogravimetric (DTG) curves (i–l) corresponding to blends B1, B2, B3, and B4, respectively.

The thermogravimetric curves with heating rates of 20 to 40 °C min^{-1} also showed a minor shift to the right of the peaks towards higher temperatures, as seen in Figure 7. However, the decomposition was similar, indicating a similar reaction mechanism for all heating rates. Numerous studies have reported similar behavior on lignocellulosic materials (SANTOS et al., 2020). This differential degradation pattern is crucial for optimizing biomass utilization in energy applications, as it directly impacts the yield and composition of biofuels generated through combustion and other thermal processes (CAI et al., 2018; TEH et al., 2021).

5.2 Numerical Modeling

5.2.1 Estimation of Activation Energy (E_α)

Figure 8 presents the E_α and A_α profiles across the explored isoconversional methods and Miura-Maki and Scott DAEM for the four blends. The general trends in Figs. 8(a–d) indicates that while the integral methods maintain consistency, the Friedman and Scott methods capture more complex changes in E_α profiles, particularly in Stage II and Stage III, where thermal degradation mechanisms shift. KAS, FWO, Starink, and Miura-Maki methods provide smoother activation energy trends due to their mathematical treatment. Nevertheless, the results remained within the same order of magnitude, demonstrating overall consistency across methods.

The Friedman method avoids oversimplified approximations of the temperature function, utilizing the direct differential form of the kinetic rate law instead (MISHRA; KUMAR; BHASKAR, 2015). Additionally, it is not constrained by the assumption of linear heating rate variations (CAI et al., 2018), offering greater flexibility in kinetic analysis. Nevertheless, unlike integral methods, the Friedman method does not make approximations of the temperature integral, making it more sensitive to experimental noise and highly sensitive to fluctuations in the reaction rate, presenting greater variability in activation energy (E_α), especially at higher conversion values (see Fig. 8).

The Scott method is the least simplified approach and applies a non-linear integral approximation to estimate the activation energy. Unlike model-free approaches such as FWO and KAS, the Scott method considers variations in reaction order throughout the conversion process. This results in higher activation energy peaks, as evidenced by the prominent peaks at $\alpha \approx 0.6{-}0.7$ (Figs. 8(a–d)), suggesting a phase transition in thermal degradation mechanism and indicating energy-intensive reaction steps.

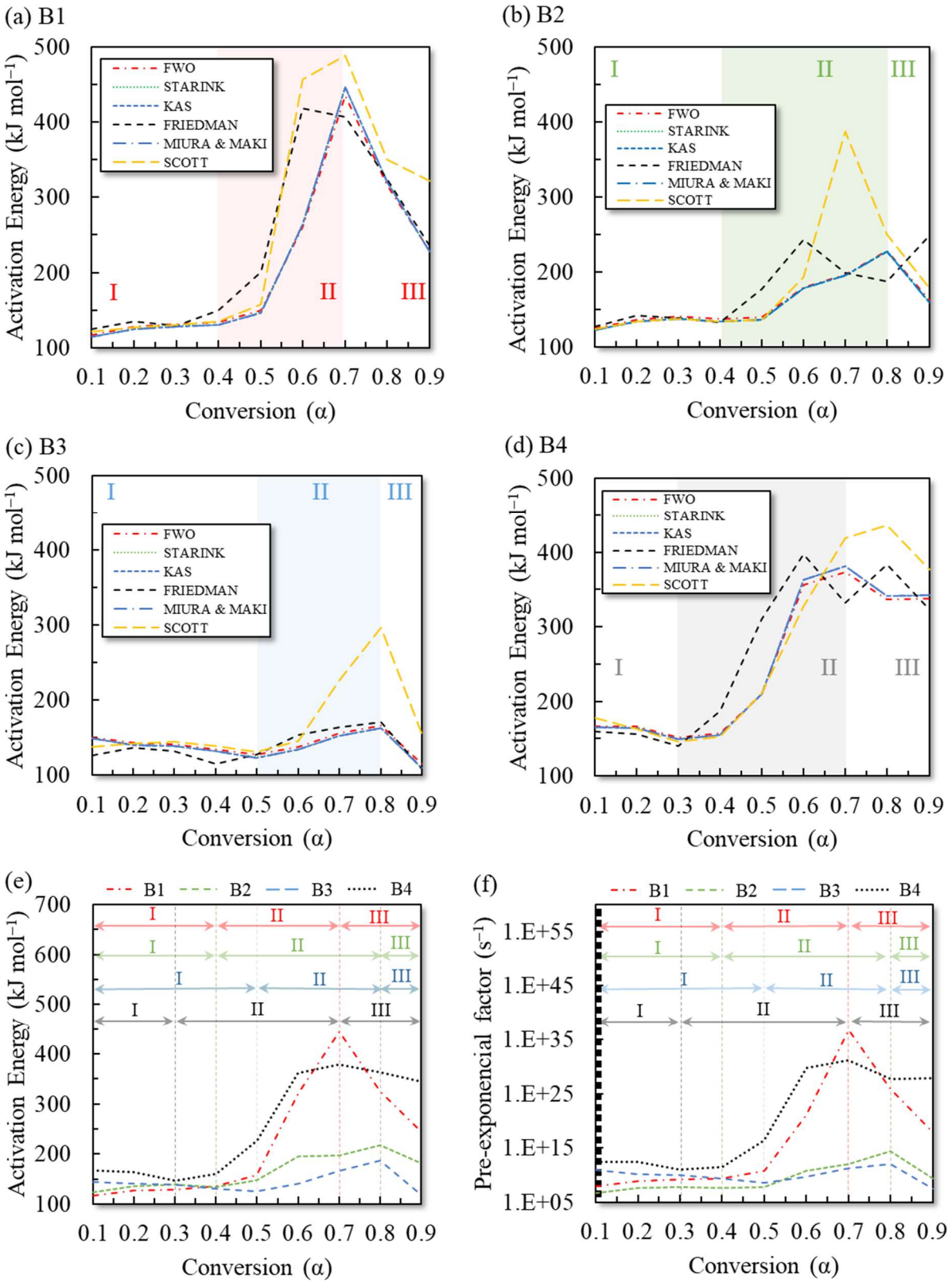

Figure 8 - Activation energy (E_α) for combustion of (a) B1, (b) B2, (c) B3, and (d) B4 determined by isoconversional methods, Miura-Maki, and Scott DAEM, (e) average activation

energy; and (f) pre-exponential factors of B1, B2, B3, and B4 based on the ASTM E698-18 standard.

Figure 8(e) presents the average activation energy for each biomass blend (B1–B4), providing insight into the distinct decomposition behaviors across three thermal degradation stages: Stage I (hemicelluloses decomposition), Stage II (cellulose degradation), and Stage III (lignin degradation and char oxidation), also depicted individually through Figs. 4(a–d). The activation energy range for Stage I is relatively low across all blends, typically between 100–180 kJ mol^{-1}, indicating the easier thermal decomposition of hemicelluloses. In Stage II, B1 and B4 exhibit the highest E_α values, exceeding 350 kJ mol^{-1}, suggesting higher cellulose crystallinity or the presence of more stable fiber components. In contrast, B2 and B3 show more moderate increases in E_α (ranging from 180–250 kJ mol^{-1}), indicative of lower resistance to thermal degradation The transition from Stage II to III is characterized by the highest E_α fluctuations, particularly for B1 and B4, where values approach 400 kJ mol^{-1}, signaling the influence of oxidative decomposition of lignin, char formation and oxidation. This trend aligns with the known behavior of biomass combustion, where recalcitrant carbonaceous structures demand greater energy for degradation, in line with Table 3.

5.2.2 Estimation of Pre-exponential Factor (A_α)

As the values of A_α are essentially unaffected by the heating rate, the average A_α for each degree of conversion (α) is displayed in Fig. 8(f), providing further insight into the kinetic complexity of each blend. The relationship between A_α and α highlights the inherent complexity of combustion reactions. The A_α parameter represents the collision frequency of reactant-activated molecules during combustion. A_α values in the Arrhenius equation typically cover a broad range (E+05 to E+20 s^{-1}) for solid-phase reactions, particularly for first-order reactions (HE et al., 2020). When A_α exceeds E+09 s^{-1}, the system demonstrates high reactivity, indicating the formation of relatively simple activated complexes. Conversely, A_α values below E+09 s^{-1} reflect lower reactivity, where surface reactions and rotational movements of activated complexes act as inhibitory factors (SIDDIQI et al., 2020). Additionally, higher A_α values indicate that combustion reactions require substantial energy input to proceed (GARCÍA-ALAMILLA, 2022). This comprehensive understanding of A_α aids in interpreting the intricate combustion process mechanisms, with significant implications for reactor and process design.

The estimated A_α values for the blends exhibited a wide range, reflecting the varying complexity of the combustion processes. For B1, the values ranged from 7.80 E+07 to 4.74 E+36 s^{-1}; for B2, they spanned from 5.46 E+06 to 2.60 E+14 s^{-1}; for B3, the values were between 2.27 E+08 and 1.30 E+12 s^{-1}; and for B4, the range extended from 1.10 E+11 to 1.50E+31s^{-1}. These results were consistent with the findings for E_α (Fig. 8(e)).

The observed increase in A_α in Stage III for B1 and B4 suggests a transition to a more complex reaction mechanism, likely influenced by secondary tar cracking and char oxidation. The lower A_α values for B2 and B3 indicate faster degradation kinetics, consistent with the lower activation energy observed in Stage II. The exponential rise in A_α for B1 and B4 at higher conversions supports the hypothesis of more thermally stable components requiring greater molecular collisions to overcome decomposition barriers (RAVEENDRAN; GANESH; KHILAR, 1996). These findings align with prior discussions and studies on biomass combustion (RAVEENDRAN; GANESH; KHILAR, 1996). This reinforces that blends with higher lignin content (such as B4) exhibit higher activation energies and pre-exponential factors in the final stages of degradation. The abrupt increase in A_α at a conversion rate of 0.5 might also be related to a disturbance near the end of conversion or the energy barrier resulting from interference by minerals in the ash (SAIT et al., 2012).

5.2.3 Three-Parallel Model – DAEM

The Three-Parallel Distributed Activation Energy Model (DAEM) was utilized to evaluate the decomposition of lignocellulosic biomass by considering three pseudo-components: hemicelluloses, cellulose, and lignin. The average values reported by CHEN et al., 2015a were used to derive initial parameter guesses for this study, which conducted a similar analysis on five other lignocellulosic biomass samples, as detailed in Table 5. Each experiment generated approximately 5,000 data points. To optimize processing time, interpolation was applied to determine temperature values at 1 °C intervals, reducing the dataset to about 700 points. This preprocessing significantly enhanced computational efficiency while maintaining data accuracy. The average results obtained for each biomass sample are summarized in Table 5, while the fitting results for TGA and DTG at a heating rate of 30 °C min^{-1} are illustrated in Figs. 9 and 10. Table 5 shows that the processing time ranged from 5 to 9 min, proving the model's efficiency. The model proves feasible for large-scale analyses with a minimal computational cost of 1.3 GB of RAM and 27.1 GB of disk space.

Table 5 - The simulation results of three-parallel-DAEM at a heating rate of 30 °C min^{-1}.

		E_i (kJ mol $^{-1}$)	σ_i (kJ mol $^{-1}$)	A_i (s^{-1})	x_i (%)	Processing (min)	MAPE (%)
IG[a]	H[b]	150.00	5.00	5.00 E+12	20.0	-	-
	C[c]	175.00	1.00	5.00 E+12	50.0	-	-
	L[d]	200.00	25.00	1.00 E+13	30.0	-	-
B1	H	156.07	9.71	4.96 E+12	15.4	5.1	3.0%
	C	170.13	3.79	4.98 E+12	47.2		
	L	209.18	10.07	1.02 E+13	37.4		
B2	H	154.59	6.63	4.97 E+12	13.1	7.1	2.5%
	C	171.50	1.33	5.00 E+12	51.6		
	L	206.81	8.64	1.03 E+13	35.2		
B3	H	158.42	9.23	5.87 E+12	20.2	8.8	3.6%
	C	175.50	1.79	1.98 E+13	44.9		
	L	203.46	9.68	1.15 E+13	33.9		
B4	H	155.77	10.11	4.92 E+12	15.8	7.6	2.2%
	C	171.08	4.19	4.99 E+12	45.1		
	L	213.19	10.45	1.12 E+13	39.1		

[a] Initial guest from CHEN et al., 2015a; [b] Hemicellulosess; [c] cellulose; [d] lignin; [e] Values considering $0.1 < \alpha < 0.9$.

As shown in Fig. 9 and Table 5, the three-parallel DAEM model strongly aligns with the experimental results, achieving a Mean Absolute Percentage Error (MAPE) between 2.2% and 3.6%, considering the conversion range between 0.1 and 0.9. Comparatively, the study by CHEN et al., 2015a reported a wider MAPE range of 37% to 69%. These findings highlight the improved consistency and reliability of the developed model and confirm its adequate fit.

Regarding the DTG curve in Fig. 10, it is evident that the model deviates slightly in regions with higher variations. These deviations can be attributed to the nature of the experimental DTG curve, which exhibits sharp, prominent peaks, whereas the simulated model relies on a specific exponential equation, making such disparities expected. Despite these differences, the model produced results within the same order of magnitude as the experimental data, with peak temperatures closely aligning.

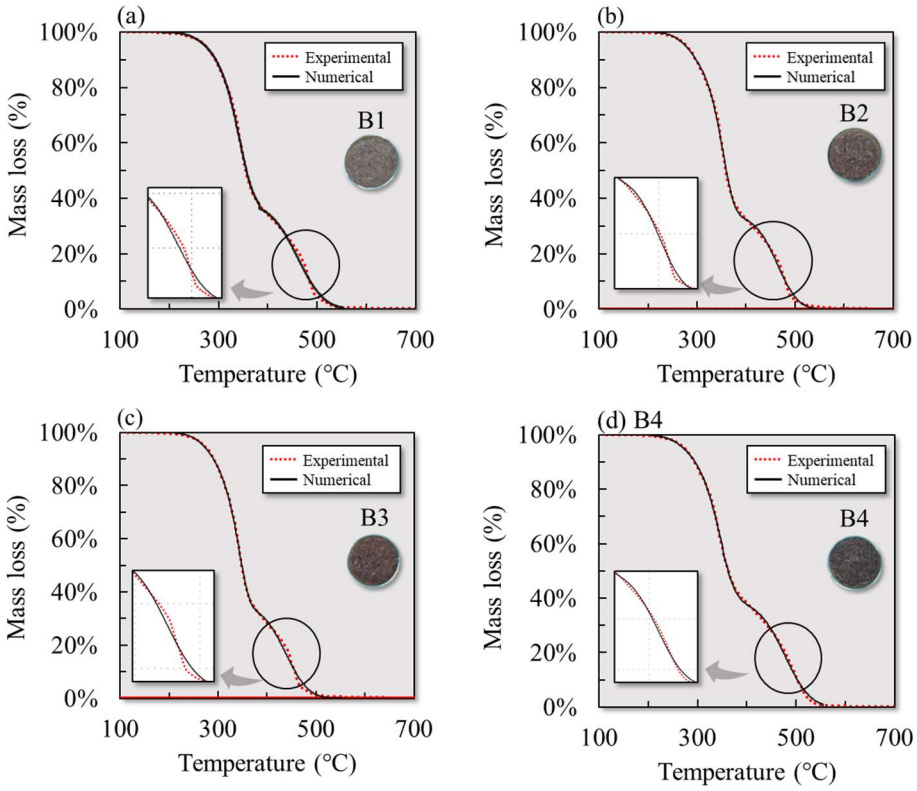

Figure 9 - Experimental mass loss and numerical prediction results of three-parallel-DAEM at 30 °C min^{-1} for (a) B1, (b) B2, (c) B3, and (d) B4 combustion.

The results obtained using the DAEM emphasize the decomposition stages of biomass components: the shoulder at lower temperatures corresponds to the decomposition of hemicelluloses, the first peak represents cellulose decomposition, and the second peak indicates lignin decomposition. These outcomes demonstrate the reliability and robustness of the proposed model in capturing the primary thermal degradation processes.

The mean activation energy (E_i) ranged from 154.59 to 158.42 kJ mol^{-1} for hemicelluloses, 170.13 to 175.50 kJ mol^{-1} for cellulose, and 203.46 to 213.19 kJ mol^{-1} for lignin, following the sequence E_i (lignin) > E_i (cellulose) > E_i (hemicelluloses). These results align with previous research and are consistent with values reported in the literature, reinforcing the reliability of the findings (CAI; WU; LIU, 2013; CHEN et al., 2015b; HU et al., 2016; VÁRHEGYI et al., 2010). This sequence reflects the relative thermal stability of the pseudo-components. This relationship correlates with the peaks observed in the DTG curve, as E_i represents the height of the potential energy barrier for a reaction; lower barriers facilitate faster and easier decomposition.

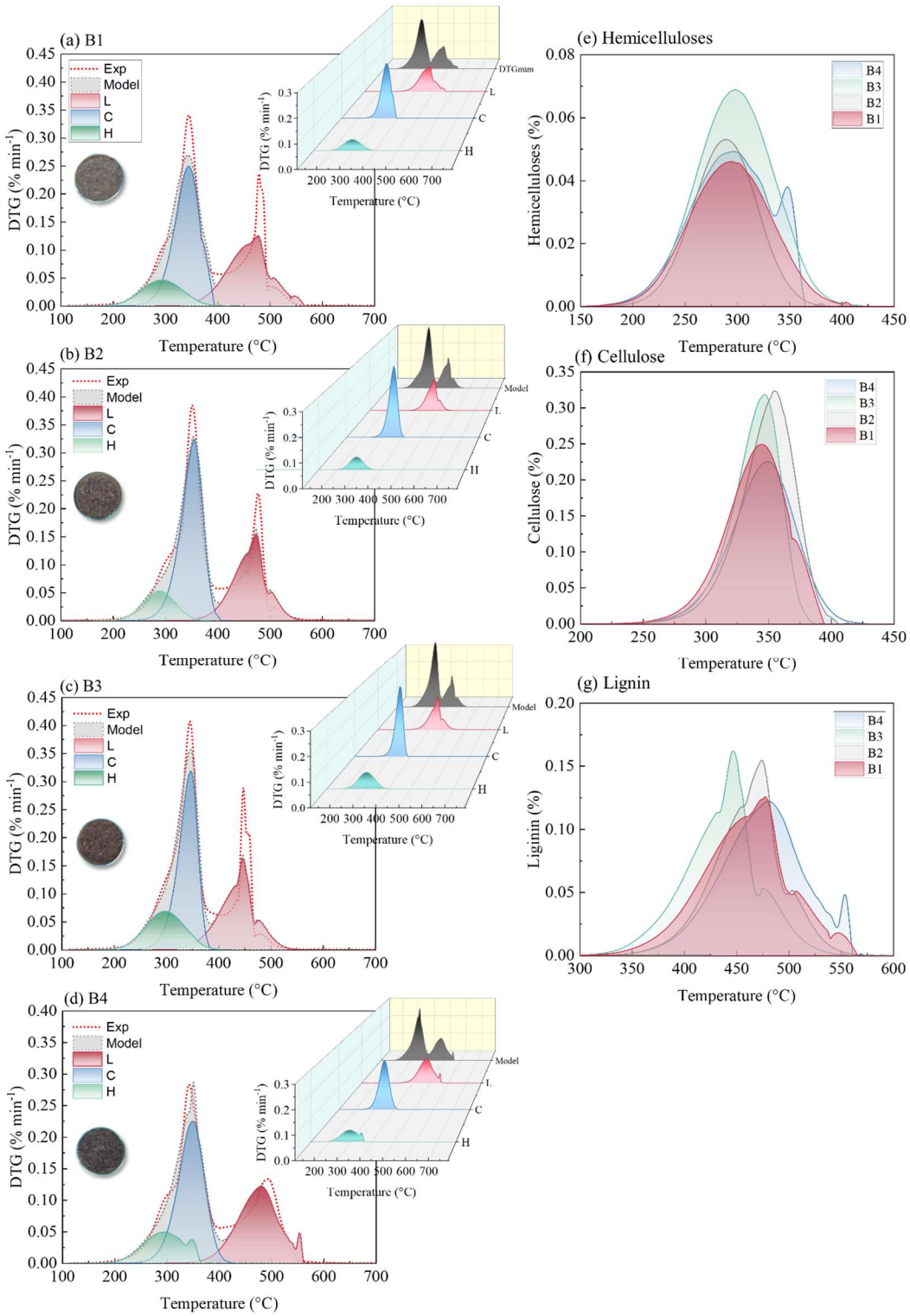

Figure 6 - Experimental and simulated derivative thermogravimetric (DTG) curves (in % min^{-1}) and deconvolution results as a function of temperature for the combustion of the biomass blends: (a) B1, (b) B2, (c) B3, and (d) B4. The comparison of deconvoluted peaks for (e) hemicelluloses, (f) cellulose, and (g) lignin is shown as a function of temperature for the proposed blends, highlighting the distinct thermal degradation profiles of each component.

The standard deviation (σ_i) of the activation energies ranged from 6.63 to 10.11 kJ mol $^{-1}$ for hemicelluloses, 1.33 to 4.19 kJ mol $^{-1}$ for cellulose, and 8.64 to 10.45 kJ mol $^{-1}$ for lignin. The standard deviation (σ_i) of the pseudo-components follows the order: σ_i (lignin) > σ_i (hemicelluloses) > σ_i (cellulose), consistent with previous studies (CAI; WU; LIU, 2013; CHEN et al., 2015a; HU et al., 2016; VÁRHEGYI et al., 2010). This indicates that lignin exhibits broader E_i distribution than hemicelluloses and cellulose. However, the σ_i values for lignin in this study are lower than those reported in the literature, likely due to the accentuation of the second peak in the DTG curve, which reduces the observed standard deviation. Nevertheless, the degradation of each component occurs within the temperature ranges reported in the literature: 220–280 °C for hemicelluloses, 240–350 °C for cellulose, and 250–500 °C for lignin (BRACHI et al., 2015; WILD; WOUTER J. J. HUIJGEN; RICHARD J.A. GOSSELINK, 2014). These results reinforce the consistency of the model with known thermal behavior.

The pre-exponential factor (A_i in Table 5) varied from 4.92 E+12 to 5.87 E+12 s^{-1} for hemicelluloses, 4.98 E+12 to 1.98 E+13 s^{-1} for cellulose, and 1.02 E+13 to 1.15 E+13 s^{-1} for lignin. These values align well with those reported in the literature (CAI; WU; LIU, 2013; CHEN et al., 2015a; HU et al., 2016; VÁRHEGYI et al., 2010). Table 5 also indicates that the estimated mass fractions for hemicelluloses, cellulose, and lignin are 13.1–20.2%, 44.9–51.6%, and 33.9–39.1%, respectively. Compared to the experimental data in Table 5, the errors range from 3% to 18%. These discrepancies may stem from the simulation's exclusion of ash and extractives (e.g., B3 contains 9%), resulting in slight deviations in the composition (SANTANA; OKINO, 2007; SHI; WANG, 2014; YAO et al., 2008). Despite these differences, the simulated results exhibit close agreement with the experimental data and values reported in the literature for other biomasses, offering strong evidence of the model’s reliability and accuracy.

5.2.4 Model Validation

The previously discussed kinetics were applied to forecast the thermogravimetric (TG) curve at three different heating rates: 25, 35, and 50 °C min^{-1} to validate the kinetic results and evaluate their capacity to predict mass degradation during biomass combustion. Figure 11 and Table 6 present results for conversions between 0.1 and 0.9, as the literature indicates that the

isoconversional and DAEM methods only find an appropriate E_α within this conversion range (VYAZOVKIN et al., 2011).

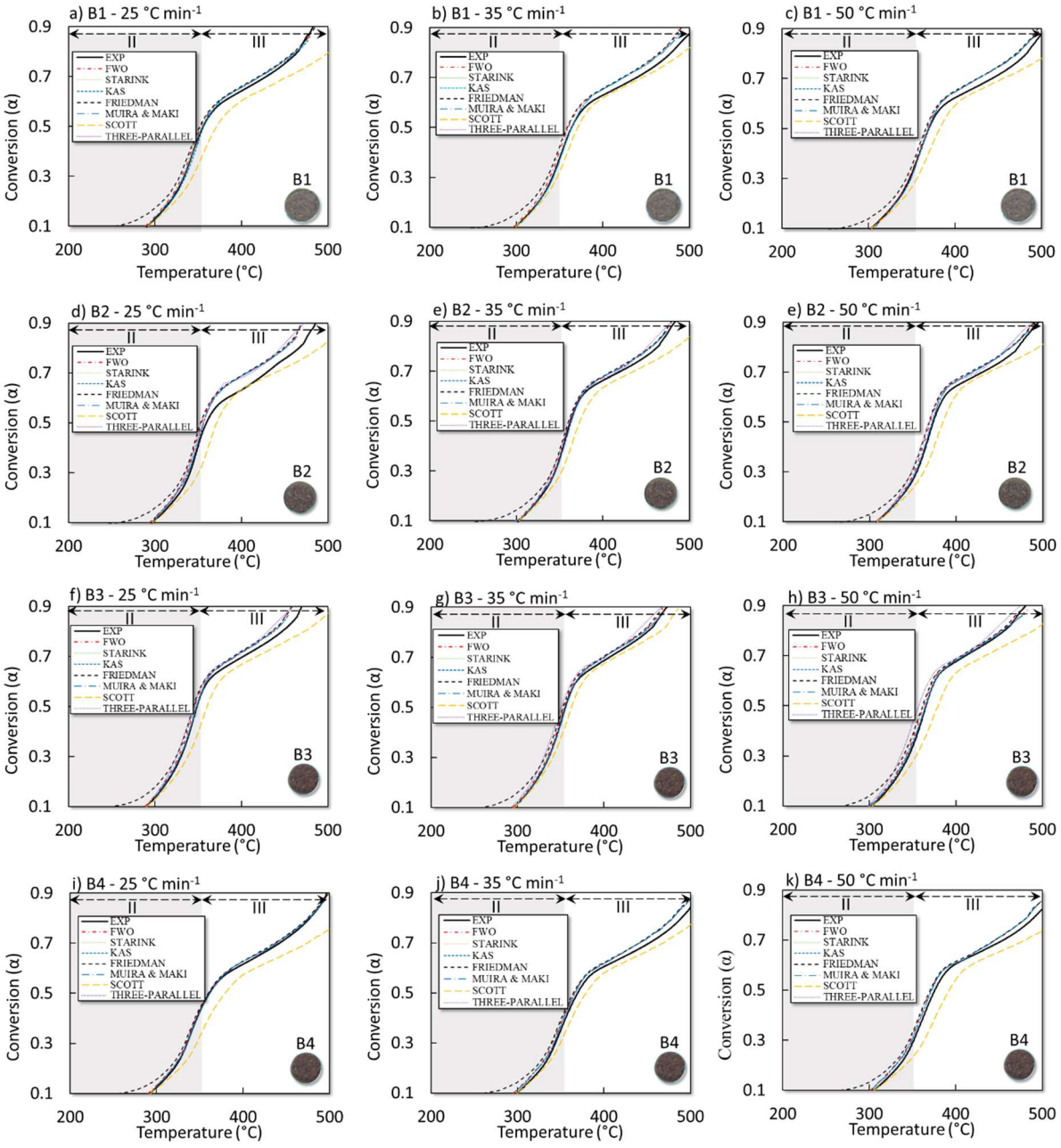

Figure 7- Prediction TG fitting for B1, B2, B3 and B4 at 25, 35, 50 °C min^{-1}.

The TG curves in Figure 11 reveal that the predicted curves for all blends and methods represent only the most significant stages. The first stage (below 200 °C) corresponds to moisture release and volatile compounds with volatilization temperatures similar to moisture. This stage cannot be represented in the predicted curves, as the model initiates at a conversion

of 0.1. However, in the subsequent stage (200–400 °C), the conversion increases from nearly zero to above 0.6 across all predicted models and blends, indicating a high volatile content and considerable thermal reactivity (BONGOMIN et al., 2024).

Table 4- Mean absolute percentage error of thermogravimetric curve predictions.

	Isoconversional				DAEM			Average
Rate [a]	**KAS**	**FWO**	**STARINK**	**FRIEDMAN**	**MM [b]**	**SCOTT**	**TP [c]**	**-**
				B1				
25	2.20%	3.73%	2.19%	8.24%	2.19%	10.92%	5.02%	**4.93%**
35	3.33%	5.73%	3.33%	10.18%	3.33%	4.86%	11.12%	**6.00%**
50	3.45%	3.56%	3.45%	8.53%	3.45%	8.06%	7.18%	**5.40%**
				B2				
25	7.30%	9.14%	7.30%	13.51%	7.30%	7.95%	15.07%	**9.65%**
35	1.86%	3.12%	1.86%	7.88%	1.86%	8.40%	6.20%	**4.45%**
50	2.72%	4.43%	2.72%	9.52%	2.72%	7.88%	9.16%	**5.59%**
				B3				
25	2.81%	4.88%	2.81%	9.78%	2.81%	8.90%	11.30%	**6.18%**
35	1.29%	3.06%	1.29%	8.07%	1.29%	5.41%	9.14%	**4.22%**
50	2.16%	3.93%	2.16%	8.58%	2.16%	10.79%	9.90%	**5.67%**
				B4				
25	1.38%	2.28%	1.38%	5.21%	1.38%	11.49%	3.77%	**3.84%**
35	4.53%	5.53%	4.53%	8.27%	4.53%	6.37%	7.31%	**5.87%**
50	4.48%	5.55%	4.48%	8.15%	4.48%	10.88%	5.42%	**6.21%**
Average	**3.13%**	**4.58%**	**3.13%**	**8.83%**	**3.13%**	**8.49%**	**8.40%**	**5.67%**

[a] (°C min^{-1}); [b] MIURA-MAKI; [c] THREE-PARALELL.

The initial DTG peaks were observed at 334–366, 344–377, 342–373, and 334–374 °C for B1, B2, B3, and B4, respectively, depending on the heating rate. Minimal variation in DTG values was noted across the methods, with the Scott method showing the largest deviation in peak temperature, with an error of 4.3% for B2. This variation is expected and does not compromise the model's predictive capability, as it remains a mathematical approximation. All methods successfully predict cellulose degradation (BRACHI et al., 2015; WILD; WOUTER J. J. HUIJGEN; RICHARD J.A. GOSSELINK, 2014).

The third stage (400–600 °C) corresponds to lignin degradation in the biomass, which the model cannot fully represent due to its limitation of a 0.9 conversion. The second DTG peaks were observed at 465–536, 464–518, 429–505, and 469–506 °C for B1, B2, B3, and B4, respectively. These peaks are associated with lignin degradation, and the differences in DTG

values were negligible, confirming that the methods can predict lignin degradation. However, the Scott method exhibited the largest deviation in peak temperature, with an error of 14.1% for B1.

Few studies have focused on predicting the combustion behavior of lignocellulosic biomass. Fawzy et al. (2022) investigated the combustion of Sesbania, a promising short-rotation woody crop, and found that a 60% conversion occurred between 400–450 °C across heating rates of 10, 20, 30, 40, and 50 °C min^{-1}, with minimal variation between rates (FAWZY et al., 2022). Similarly, Osman et al. (2020) examined the non-isothermal combustion of blackberry pomace at high heating rates (20, 50, 75, and 100 °C min^{-1}) and observed accelerated reactions at higher temperatures (OSMAN et al., 2020) .

Table 6 presents the predictions' mean absolute percentage error (MAPE). It is observed that the lowest error (1.29%) occurred for B3 at a heating rate of 35 °C min^{-1} using the KAS, STARINK, and MIURA-MAKI methods, while the highest error (15.07 %) was observed for B2 at a heating rate of 25 °C min^{-1} using the three-parallel-DAEM method. The KAS, STARINK, and MIURA-MAKI methods generally provided the most accurate degradation predictions. These similar values arise because these equations are quite similar, resulting in thermodynamic parameters and conversion values that are also very close. On the other hand, the highest errors were associated with FRIEDMAN, SCOTT, and three-parallel–DAEM methods due to the complexity of their mathematical resolution.

Despite these differences, the average error of 5.79% suggests that isoconversional and DAEM methods can reliably predict the mass degradation of lignocellulosic biomass. Non-isothermal predictions offer valuable insights for academia and industry, enabling the identification of optimal operational parameters such as temperature and heating rate, significantly enhancing process engineering (OSMAN et al., 2020).

5.3 Thermodynamic Analysis

Evaluating thermodynamic parameters is essential for assessing the feasibility of combustion processes and conducting energy analyses (PRAKASH; ABHISEK; SACHIN, 2021). Since the heating rate has a negligible effect on the thermodynamic parameters (Rammohan et al., 2022), Fig. 12 presents the average thermodynamic parameters for all biomass blends, determined at a heating rate of 30 °C min^{-1} using four isoconversional methods, and the Miura-Maki and Scott DAEM approaches.

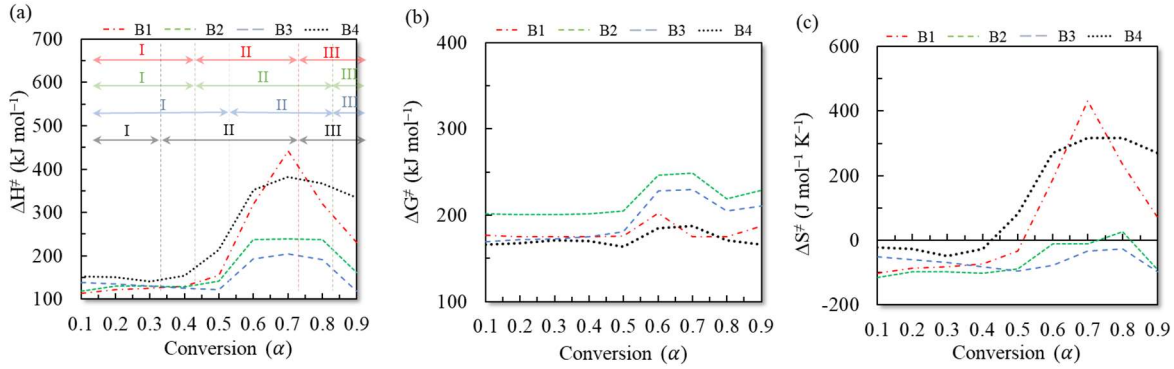

Figure 8- Thermodynamic parameters ($\Delta H^{\neq}$, $\Delta S^{\neq}$, and $\Delta G^{\neq}$) for all biomass blends (B1, B2, B3, and B4), highlighting their variations across the conversion range.

The enthalpy change ($\Delta H^{\neq}$) represents the energy required to transition from reactants to the activated complex (RIAZ; OLUWOYE; AL-ABDELI, 2022; VYAZOVKIN, 2024). Figure 12(a) shows the $\Delta H^{\neq}$ values ranging from 112.9–441.9 kJ mol^{-1} for B1, 119.2–238.7 kJ mol^{-1} for B2, 119.3–204.1 kJ mol^{-1} for B3, and 140.4–382.7 kJ mol^{-1} for B4 as a function of the conversion rate, reflecting the diverse energy requirements for biomass decomposition and aligned with the distinctive stages of the E_α (Fig. 8(e)). At lower conversion levels ($\alpha < 0.5$), all blends exhibit relatively stable $\Delta H^{\neq}$ values, ranging from 112.89 to 213.43 kJ mol^{-1}. However, beyond this threshold, $\Delta H^{\neq}$ increased notably, indicating higher energy demands for bond dissociation and implying the dominance of lignin decomposition at higher conversion (VYAZOVKIN, 2024).

The Gibbs free energy change ($\Delta G^{\neq}$) quantifies the energy barrier for the formation of the activated complex, as illustrated in Fig. 12(b). Across the conversion range, $\Delta G^{\neq}$ remained relatively stable, varying from 175.0–202.9 kJ mol^{-1} for B1, 200.5–248.6 kJ mol^{-1} for B2, 169.3–229.6 kJ mol^{-1} for B3, and 163.3–187.4 kJ mol^{-1} for B4, confirming the non-spontaneous nature of combustion reactions and the influence of biomass composition on energy barriers. The consistently positive $\Delta G^{\neq}$ values indicate that the formation of the activated complex in these biomass blends is non-spontaneous, a common characteristic of combustion reactions (GARCÍA-ALAMILLA, 2022).

The entropy change $\Delta S^{\neq}$ serves as an indicator of system reactivity and molecular disorder during the transition state (ALVES et al., 2022b). Figure 12(c) present the variation of $\Delta S^{\neq}$ values as a function of α for the four blends. The entropy values ranged from –103.13 to 431.54, –116.31 to 27.48, –96.58 to –26.93, and –49.60 to 316.95 J mol^{-1} K^{-1} for B1, B2, B3,

and B4, respectively. Negative $\Delta S^{\neq}$ values are more prevalent in reactions with high molecularity, where multiple reactant molecules coalesce into a single activated complex, signifying lower disorder and prolonged reaction times (MUMBACH et al., 2022). The negative $\Delta S^{\neq}$ values observed for B2 and B3 suggest a lower degree of disorder in the activated complex, implying that these reactions are closer to thermodynamic activation equilibrium, enhancing stability (MUMBACH et al., 2022). Conversely, for B1 and B4, $\Delta S^{\neq}$ shifts from negative to positive at approximately 0.5 conversion, signifying that the disorder in the activated complex surpasses that of the reactants, thereby moving the system away from activation equilibrium (ALVES et al., 2022b).

Comparatively, studies on the combustion of Pinus wood by Xu et al. (2021) and Chen et al. (2020) report $\Delta H^{\neq}$ values similar to those of B2 and B3, and $\Delta G^{\neq}$ values consistent with all the blends analyzed in this work, corroborating the thermodynamic behavior observed (CHEN et al., 2020; XU; PAN; CHEN, 2021). Furthermore, the combustion of *Lycium barbarum*, an abundant biomass widely used in the pharmaceutical and food industries, exhibited $\Delta H^{\neq}$ and $\Delta S^{\neq}$ values comparable to those of B1 and B4 (CHEN et al., 2024). These observations reinforce the influence of biomass composition on thermodynamic parameters, demonstrating that despite similarities in certain properties, the diversity in $\Delta S^{\neq}$ behavior highlights different lignocellulosic materials' unique reactivity and decomposition mechanisms under thermal conditions.

5.4 CO_2 Uptake and Potential Emissions

An essential attribute of biomass feedstock as a renewable fuel is its capacity for CO_2 uptake during growth, which offsets emissions from combustion (Alves et al., 2020; Maj, 2018). The CO_2 uptake promoted by the feedstock and estimated emission factors (expressed in kilograms per ton of biomass) are presented in Fig. 13 B1, B2, B3, and B4's CO_2 uptake values were 1.729, 1.743, 1.776, and 1.677 tons, respectively, corresponding to carbon contents of 47.15%, 47.53%, 48.43%, and 45.74%.

B3 demonstrated the highest CO_2 emissions, whereas B4 recorded the lowest, with a difference of 5.87%. Regarding NOx emissions, B4 recorded the highest value, although still within relatively low levels. This NO_x emission level was slightly higher than biomasses such as *Pinus radiata*, *Eucalyptus globulus*, and *Nothofagus obliqua* but lower than wheat straw, oat

grain, larch needles, and rapeseed pods (Cereceda-Balic et al., 2017; Maj, 2018). Sulfur dioxide emissions were negligible, and the emission factors for the blends were lower than those reported in other studies (Alves et al., 2020; Cereceda-Balic et al., 2017; Luiz et al., 2022; Maj, 2018; Maj et al., 2019). B4 demonstrated the lowest overall emissivity among the evaluated biomasses, indicating its suitability for reducing NO_x and SO_2 emissions when used as fuel.

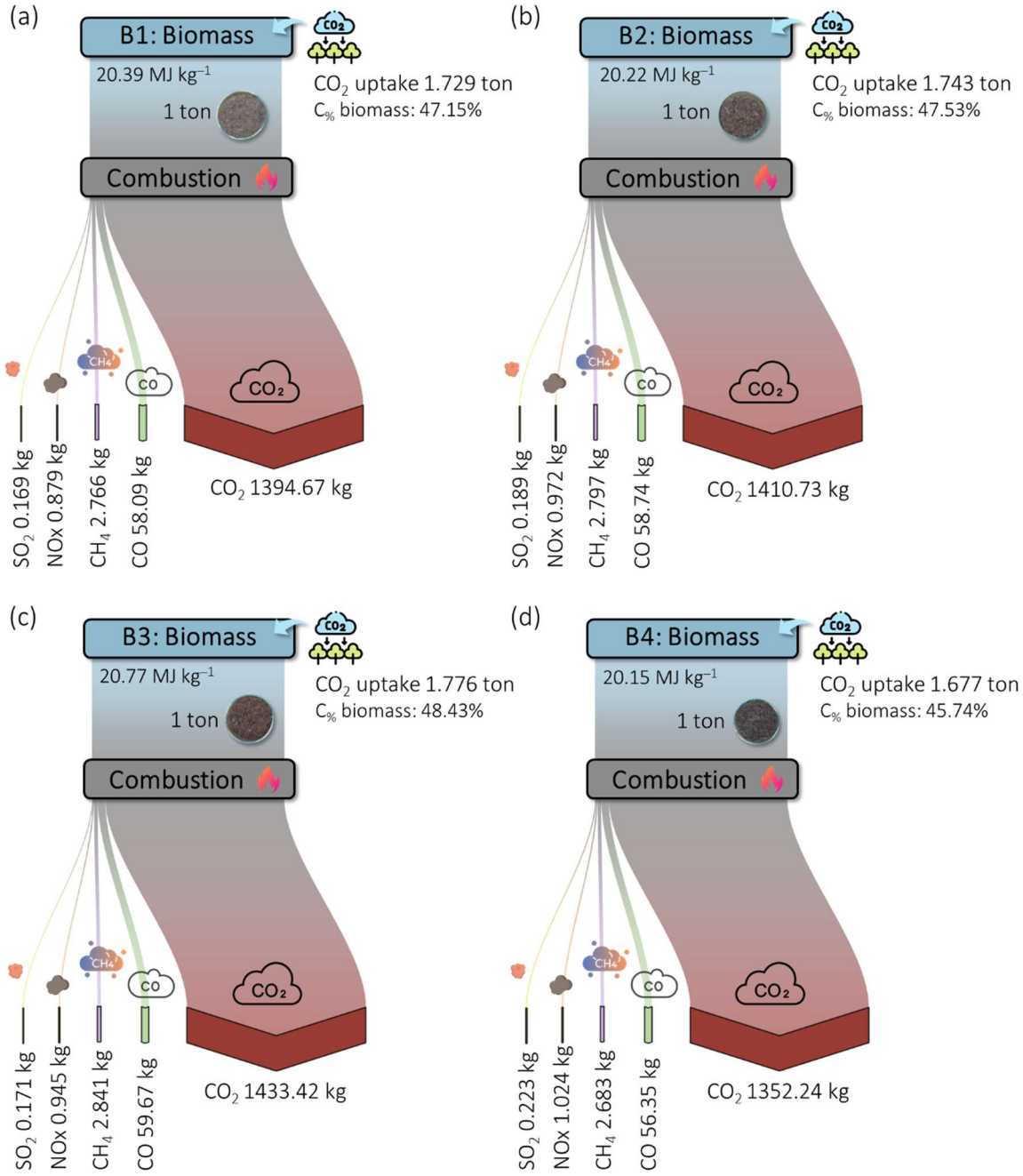

Figure 9 - The Sankey diagram of combustion emissions (relative to 1 ton of biomass) and CO_2 uptake four the blends (a) B1, (b) B2, (c) B3, and (d) B4.

The emission factors for the biomass feedstocks (B1, B2, B3, and B4) per megajoule (MJ) of energy are also presented in Table 7, along with literature on agro-forest residues and fossil fuels for comparison. The related emissions demonstrate a notable environmental advantage compared to fossil fuels and some agro-residues. These results are particularly significant when considering their alignment with global efforts to reduce greenhouse gas emissions in energy production systems.

Table 5 - Comparison of emission factors in terms of energy (tons of emission per MJ) for B1, B2, B3 and B4 with other feedstocks.

Feedstock		**HHV** [a]	E_{CO} [b]	E_{CO_2} [b]	E_{NOx} [b]	E_{SO_2} [b]	E_{CH_4} [b]	**Ref.**
Biofuel								
Agro-residues Amazon [c]	AS	19.18	3.113	76.241	0.217	0.010	0.148	(DA COSTA et al., 2023)
	CPH	17.69	3.100	75.909	0.393	0.018	0.148	
	CH	18.54	3.073	75.261	0.234	0.024	0.146	
	MC	19.65	3.072	75.216	0.341	0.014	0.146	
	PEFB	18.35	3.013	73.787	0.256	0.008	0.143	
Agro-residues (*Jackfruit*)	Peel	16.27	3.090	73.968	0.286	0.045	0.147	(ALVES et al., 2020b)
	Seed	17.15	3.001	71.862	0.508	0.042	0.143	
Torrefied Amazon wood waste	AB *	20.22	2.905	69.773	0.056	0.008	0.138	(SILVEIRA et al., 2025)
	AB_{225}	20.47	2.995	71.983	0.051	0.009	0.143	
	AB_{250}	20.66	3.072	73.876	0.036	0.009	0.146	
	AB_{275}	21.64	3.315	79.899	0.050	0.009	0.158	
Amazon wood waste	B1	20.39	2.849	68.400	0.043	0.008	0.136	Study
	B2 *	20.22	2.905	69.773	0.056	0.008	0.138	
	B3	20.77	2.873	69.014	0.046	0.008	0.137	
	B4	20.15	2.797	67.109	0.051	0.011	0.133	
Fossil Fuel								
Coal	LRC	21.42	3.673	88.659	0.148	0.047	0.175	(ZHUANG et al., 2019)
	MRC	28.12	3.084	74.536	0.147	0.053	0.147	
	HRC	27.23	3.432	83.030	0.124	0.030	0.163	
Diesel		42.80	0.210	73.830	0.720	0.047	0.007	(INTERGOVERNMENTAL PANEL ON CLIMATE CHANGE, 2019)

[a] MJ kg^{-1} ; [b] (ton MJ^{-1}). [c] AS – Açaí seed, CH – coconut husk, CPH – cocoa pod husk, PEFB – palm empty fruit bunch, and MC – maize cob;

In terms of agro-residues, the studied feedstocks show significant advantages. Emission factors for agro-residues such as jackfruit seed and peel are slightly higher in CO and CO_2

emissions (3.001–3.090 tons CO MJ^{-1} and 71.862–73.968 tons CO_2 MJ^{-1}) compared to B1–B4. Furthermore, other agro-residues like cocoa pod husk (CPH) and coconut husk (CH) produce higher NO_x, SO_2, and CH_4 levels, demonstrating that B1–B4 provides a more favorable environmental profile for sustainable energy production.

Compared to fossil fuels, the benefits of B1–B4 become even more pronounced. Fossil fuels such as low-rank coal (LRC) exhibit substantially higher emissions of CO (3.673 tons MJ^{-1}) and CO_2 (88.659 tons MJ^{-1}), reaffirming the environmental benefits of using biomass feedstocks. Emission analysis revealed mixed results when compared to diesel. CO emissions from the biomass blends ranged from 2.797 to 2.905 tons MJ^{-1}, representing a substantially higher emission than diesel's 0.210 tons MJ^{-1}. However, biomass combustion demonstrated clear environmental advantages in other aspects: CO_2 emissions were 6.5–9.1% lower, SO_2 emissions were reduced by 92.2–94.0%, and NOx emissions showed a drastic reduction of 98.5–98.9% compared to diesel.

Among the evaluated feedstocks, B4 exhibited the lowest emissions of CO (2.797 tons MJ^{-1}), CO_2 (67.109 tons MJ^{-1}), and CH_4 (0.133 tons MJ^{-1}), representing reductions of 1.8–3.7% in CO, 1.9–3.8% in CO_2, and 2.2–3.6% in CH_4 compared to B1, B2, and B3, making it particularly suitable for reducing greenhouse gas emissions. B1 also demonstrated relatively low emissions, with CO and CO_2 values 1.9% and 1.9% higher than B4, respectively. In contrast, B2 and B3 presented slightly higher CO and CO_2 emissions than B1 but exhibited lower NOx emissions, reinforcing their versatility for different energy applications.

Future research should prioritize detailed experimental assessments of biomass combustion emissions, utilizing advanced analytical techniques such as gas chromatography-mass spectrometry (GC-MS) to accurately quantify all gases emitted during incomplete combustion (Loebel Roson et al., 2024). Additionally, using a cone calorimeter should be considered to evaluate key combustion parameters, including heat release rate, total heat release, and gas production under controlled thermal radiation conditions (Chaudhuri et al., 2025). This approach would overcome the limitations of model-based estimations and provide more robust data on the composition of released gases, including volatile hydrocarbons and incomplete oxidation compounds. Additionally, the CO_2 uptake balance should be refined by considering more precise harvest cycle models tailored to specific biomes and biomass types, particularly from Amazon, ensuring that carbon sequestration is accounted for in a way that accurately reflects the long-term impact of bioenergy (Liu et al., 2018). Another promising avenue involves monetizing carbon credits, particularly within the context of Decarbonization

Credits (CBIOs) in Brazil, which represents a strategic opportunity to finance and accelerate the transition to more sustainable bioenergy systems (Brazil,2017). By integrating advanced methodologies and economic incentives, bioenergy can become a more viable renewable alternative, contributing to net carbon emission reductions and the decarbonization of the energy sector.

6 CONCLUSION

The results of this study emphasize the viability of utilizing Amazon wood residues as a renewable energy source for decentralized systems, providing a sustainable alternative to fossil fuels in remote communities. Comprehensive kinetic and thermodynamic analyses demonstrated that these biomass blends possess favorable combustion properties, with activation energy values reflecting efficient thermal decomposition. Furthermore, integrating advanced modeling approaches strengthened the reliability of combustion predictions, enabling better optimization of bioenergy applications.

From an environmental perspective, the studied biomass blends exhibited significant potential for emissions reduction, particularly in minimizing greenhouse gases and pollutants such as CO_2, SO_2, and NOx. The CO_2 uptake capacity of biomass further reinforces its role in offsetting emissions, aligning with global decarbonization efforts and contributing to circular bioeconomy strategies. These findings indicate that the strategic use of forest residues can enhance energy security, reduce dependence on diesel-based systems, and support the transition towards cleaner energy solutions in Amazon. Further research should assess combustion efficiency and ash-related issues on specific technologies for decentralized systems.

Future research should explore the long-term sustainability of biomass energy integration, considering supply chain logistics, economic feasibility, and life cycle assessments. Additionally, further advancements in combustion technologies and co-firing strategies could enhance biomass utilization efficiency while mitigating operational challenges. This study contributes to the broader discourse on sustainable energy transitions and climate action in tropical regions by fostering the adoption of bio-based energy solutions. The developed methodology could also be applied to various biomass sources in Brazil facing challenges of energy injustice and decentralization, such as those in the Caatinga and Cerrado regions, warranting an assessment of their local biomass potential.

REFERENCES

ALVES, J. L. F. et al. Exploring Açaí Seed (Euterpe oleracea) Pyrolysis Using Multi-component Kinetics and Thermodynamics Assessment Towards Its Bioenergy Potential. 2020a.

ALVES, J. L. F. et al. Insights into the bioenergy potential of jackfruit wastes considering their physicochemical properties, bioenergy indicators, combustion behaviors, and emission characteristics. **Renewable Energy**, v. 155, p. 1328–1338, ago. 2020b.

ALVES, J. L. F. et al. Potential of macauba endocarp (Acrocomia aculeate) for bioenergy production: Multi-component kinetic study and estimation of thermodynamic parameters of activation. **Thermochimica Acta**, v. 708, n. December 2021, 2022a.

ALVES, J. L. F. et al. Assessing the bioenergy potential of high-ash anaerobic sewage sludge using pyrolysis kinetics and thermodynamics to design a sustainable integrated biorefinery. **Biomass Conversion and Biorefinery**, v. 12, n. 3, p. 693–704, 2022b.

ALVES, J. L. F. et al. Upgrading of banana leaf waste to produce solid biofuel by torrefaction: physicochemical properties, combustion behaviors, and potential emissions. **Environmental Science and Pollution Research**, v. 29, n. 17, p. 25733–25747, 30 abr. 2022c.

ALVES, J. L. F. et al. Evaluating the bioenergy potential of cupuassu shell through pyrolysis kinetics, thermodynamic parameters of activation, and evolved gas analysis with TG/FTIR technique. **Thermochimica Acta**, v. 711, n. January, p. 179187, maio 2022d.

ARAUJO, R. O. et al. Renewable Energy from Biomass: an Overview of the Amazon Region. **Bioenergy Research**, n. 2, p. 834–849, 2021.

ARENAS, C. N.; NAVARRO, M. V.; MARTÍNEZ, J. D. Pyrolysis kinetics of biomass wastes using isoconversional methods and the distributed activation energy model. **Bioresource Technology**, v. 288, n. March, p. 121485, 2019.

BARONI, É. D. G. et al. The applicability of isoconversional models in estimating the kinetic parameters of biomass pyrolysis. **Journal of Thermal Analysis and Calorimetry**, v. 123, n. 2, p. 909–917, 2016.

BARZEGAR, R. et al. TGA and kinetic study of different torrefaction conditions of wood biomass under air and oxy-fuel combustion atmospheres. **Journal of the Energy Institute**, v. 93, n. 3, p. 889–898, 2020.

BASU, P. **Biomass Gasification, Pyrolysis and Torrefaction**. [s.l: s.n.].

BONGOMIN, O. et al. Comprehensive thermal properties, kinetic, and thermodynamic analyses of biomass wastes pyrolysis via TGA and Coats-Redfern

methodologies. **Energy Conversion and Management: X**, v. 24, n. September, p. 100723, 2024.

BOUBACAR LAOUGÉ, Z.; MERDUN, H. Kinetic analysis of Pearl Millet (Penissetum glaucum (L.) R. Br.) under pyrolysis and combustion to investigate its bioenergy potential. **Fuel**, v. 267, n. October 2019, p. 117172, 2020.

BRACHI, P. et al. Isoconversional kinetic analysis of olive pomace decomposition under torrefaction operating conditions. **Fuel Processing Technology**, v. 130, n. C, p. 147–154, 2015.

BRAZIL. LEI Nº 11.284. . 2006.

BRAZIL. National Solid Waste Policy (Law no 12.305/2010). . 2010.

CAI, J. et al. Processing thermogravimetric analysis data for isoconversional kinetic analysis of lignocellulosic biomass pyrolysis: Case study of corn stalk. **Renewable and Sustainable Energy Reviews**, v. 82, n. September 2017, p. 2705–2715, fev. 2018.

CAI, J.; WU, W.; LIU, R. Isoconversional kinetic analysis of complex solid-state processes: Parallel and successive reactions. **Industrial and Engineering Chemistry Research**, v. 51, n. 49, p. 16157–16161, 2012.

CAI, J.; WU, W.; LIU, R. Sensitivity analysis of three-parallel-DAEM-reaction model for describing rice straw pyrolysis. **Bioresource Technology**, v. 132, p. 423–426, 2013.

CAI, J.; WU, W.; LIU, R. An overview of distributed activation energy model and its application in the pyrolysis of lignocellulosic biomass. **Renewable and Sustainable Energy Reviews**, v. 36, p. 236–246, 2014.

CERECEDA-BALIC, F. et al. Emission factors for PM2.5, CO, CO2, NOx, SO2 and particle size distributions from the combustion of wood species using a new controlled combustion chamber 3CE. **Science of the Total Environment**, v. 584–585, n. x, p. 901–910, 2017.

CHEN, L. et al. Combustion behaviors of Lycium barbarum L.: Kinetics, thermodynamics, gas emissions, and optimization. **Biomass Conversion and Biorefinery**, n. 0123456789, 2024.

CHEN, R. et al. Combustion characteristics, kinetics and thermodynamics of Pinus Sylvestris pine needle via non-isothermal thermogravimetry coupled with model-free and model-fitting methods. **Case Studies in Thermal Engineering**, v. 22, n. August, p. 100756, 2020.

CHEN, Z. et al. Characteristics and kinetic study on pyrolysis of five lignocellulosic

biomass via thermogravimetric analysis. **Bioresource Technology**, v. 192, p. 441–450, 2015a.

CHEN, Z. et al. Characteristics and kinetic study on pyrolysis of five lignocellulosic biomass via thermogravimetric analysis. **Bioresource Technology**, v. 192, p. 441–450, 1 set. 2015b.

COLPANI, D. et al. Bioenergy potential analysis of Brazil nut biomass residues through pyrolysis: Gas emission, kinetics, and thermodynamic parameters. **Cleaner Chemical Engineering**, v. 1, p. 100002, mar. 2022.

DA COSTA, J. S. et al. Relating features and combustion behavior of biomasses from the Amazonian agroforestry chain. **Biomass Conversion and Biorefinery**, v. 13, n. 1, p. 321–341, 2023.

DE OLIVEIRA, P. F. et al. Decarbonization Potential of Bioenergy Amazonian Isolated Systems: an Environmental Life Cycle Inventory. **European Biomass Conference and Exhibition Proceedings**, n. June, p. 305–312, 2024.

EPE. Potencial energético de resíduos florestais do manejo sustentável e de resíduos da industrialização da madeira. p. 1–64, 2018.

FAWZY, S. et al. Kinetic modelling for pyrolytic conversion of dedicated short rotation woody crop with predictions for isothermal, non-isothermal and stepwise heating regimes. **Applications in Energy and Combustion Science**, v. 9, n. December 2021, p. 100048, 2022.

FLORES, J. A. et al. Inventory data on Brazilian Amazon′s non-wood native biomass sources for bioenergy production. **Data in Brief**, v. 20, p. 1935–1941, 2018.

FLYNN, J. H.; WALL, L. A. A quick, direct method for the determination of activation energy from thermogravimetric data. **POLYMER LETTERS**, v. 4, p. 323–328, 1965.

FRIEDMAN, H. L. Kinetics of Thermal Degradation of Char-Forming Plastics from Thermogravimetry . Application to a Phenolic Plastic. **JOURNAL OF POLYMER SCIENCE: PART C**, n. 6, p. 183–195, 1964.

GARCÍA-ALAMILLA, P. Bioresource Technology Comparative pyrolysis studies of lignocellulosic biomasses : Online gas quantification , kinetics triplets , and thermodynamic parameters of the process Ver o. v. 346, n. December 2021, 2022.

HE, Y. et al. Characterization of Cornstalk and Bituminous Coal Based on Kinetic and Thermodynamic Parameter for Co-pyrolysis. **IOP Conference Series: Earth and Environmental Science**, v. 555, n. 1, p. 012001, 1 ago. 2020.

HEYA, M. N. et al. Elemental composition and flue gas emissions of different components from five semi-arid woody species in pyrolysed and non-pyrolysed material. **Sustainability (Switzerland)**, v. 11, n. 5, 2019.

HU, J. et al. Combustion behaviors of three bamboo residues: Gas emission, kinetic, reaction mechanism and optimization patterns. **Journal of Cleaner Production**, v. 235, p. 549–561, 2019.

HU, M. et al. Thermogravimetric kinetics of lignocellulosic biomass slow pyrolysis using distributed activation energy model, Fraser-Suzuki deconvolution, and iso-conversional method. **Energy Conversion and Management**, v. 118, p. 1–11, 2016.

IBÁ. **Relatório anual 2023**. [s.l: s.n.].

INTERGOVERNMENTAL PANEL ON CLIMATE CHANGE. Overview. **2019 Refinement to the 2006 IPCC Guidelines for National Greenhouse Gas InventorieS**, v. 2, p. 5–13, 2019.

ITTO. **Biennial review and assessment of the world timber situation 2019-2020**. [s.l: s.n.].

KATNIĆ, Đ. et al. Characterization and kinetics of thermal decomposition behavior of plum and fig pomace biomass. **Journal of Cleaner Production**, v. 352, n. April, 2022.

KIM, S.; EOM, Y. Estimation of kinetic triplet of cellulose pyrolysis reaction from isothermal kinetic results. **Korean Journal of Chemical Engineering**, v. 23, n. 3, p. 409–414, 2006.

KISSINGER, H. E. Variation of peak temperature with heating rate in differential thermal analysis. **Journal 0 f Research of the National Bureau of Standards**, v. 57, n. 4, p. 217–221, 1956.

KRISTANTO, J. et al. Kinetic Study on The Slow Pyrolysis of Isolated Cellulose and Lignin from Teak Sawdust. **Thermochimica Acta**, v. 711, n. December 2021, p. 179202, 2022.

KUMAR, S.; NAYAN, N. K.; SINGH, R. K. Kinetics of the Pyrolysis and Combustion Characteristics of Non-edible Oilseeds (Karanja and Neem Seed) Using Thermogravimetric Analysis. **http://dx.doi.org/10.1080/15567036.2012.748106**, v. 37, n. 21, p. 2352–2359, 2 nov. 2015.

LIMA, M. D. R. et al. Charcoal of logging wastes from sustainable forest management for industrial and domestic uses in the Brazilian Amazonia. **Biomass and Bioenergy**, v. 142, n. October, 2020a.

LIMA, M. D. R. et al. Logging wastes from sustainable forest management as

alternative fuels for thermochemical conversion systems in Brazilian Amazon. **Biomass and Bioenergy**, v. 140, p. 105660, 1 set. 2020b.

LIU, H. et al. Three pseudo-components kinetic modeling and nonlinear dynamic optimization of Rhus Typhina pyrolysis with the distributed activation energy model. **Applied Thermal Engineering**, v. 157, 5 jul. 2019.

LOPES, F. C. R.; PEREIRA, J. C.; TANNOUS, K. Thermal decomposition kinetics of guarana seed residue through thermogravimetric analysis under inert and oxidizing atmospheres. **Bioresource Technology**, v. 270, n. June, p. 294–302, 2018.

LOPES, F. C. R.; TANNOUS, K.; RUEDA-ORDÓÑEZ, Y. J. Combustion reaction kinetics of guarana seed residue applying isoconversional methods and consecutive reaction scheme. **Bioresource Technology**, v. 219, p. 392–402, 2016.

LUZ, E. DA S. et al. Challenges of the lumber production in the Amazon region: relation between sustainability of sawmills, process yield and logs quality. **Environment, Development and Sustainability**, v. 23, n. 4, p. 4924–4948, 2021.

MAJ, G. Emission factors and energy properties of agro and forest biomass in aspect of sustainability of energy sector. **Energies**, v. 11, n. 6, 2018a.

MAJ, G. Emission Factors and Energy Properties of Agro and Forest Biomass in Aspect of Sustainability of Energy Sector. **Energies**, v. 11, n. 6, p. 1516, 11 jun. 2018b.

MAJ, G. et al. Estimation of energy and emissions properties of waste from various species of mint in the herbal products industry. **Energies**, v. 13, n. 1, 2019.

MILOS˘ RADOJEVIĆ et al. Comparative pyrolysis kinetics of various biomasses based on model-free and DAEM approaches improved with numerical optimization procedure. **PLoS ONE 13**, p. 1–25, 2018.

MISHRA, G.; KUMAR, J.; BHASKAR, T. Kinetic studies on the pyrolysis of pinewood. **Bioresource Technology**, v. 182, p. 282–288, 2015.

MIURA, K.; MAKI, T. A simple method for estimating f(E) and k0(E) in the distributed activation energy model. **Energy and Fuels**, v. 12, n. 5, p. 864–869, 1998.

MMAMC. **Floresta Nacional de Jacundá (RO)**.

MME. **Balanço energético nacional**. [s.l: s.n.].

MME. **Boletim Mensal de Monitoramento do Sistema Elétrico Brasileiro**. [s.l: s.n.]. Disponível em: <http://www.mme.gov.br/web/guest/secretarias/energia-eletrica/publicacoes/boletim-de-monitoramento-do-sistema-eletrico?_20_displayStyle=descriptive&p_p_id=20>.

MOREIRA, M. G.; RODRIGUES, P. P. DE O.; SILVEIRA, E. A. Comprehensive Developments of the Distributed Activation Energy Model (Daem) for Determining Pyrolysis Kinetic Parameters of Biomass Residues. **European Biomass Conference and Exhibition Proceedings**, n. June, p. 762–768, 2024.

MOREIRA, M. G.; RODRIGUES, P. P. O.; SILVEIRA, E. A. ISOCONVERSIONAL MODELING FOR DETERMINING PYROLYSIS KINETIC AND THERMODYNAMIC PARAMETERS OF BIOMASS RESIDUES. **27th ABCM International Congress of Mechanical Engineering**, 2023.

MORTARI, D. A. et al. Co-firing of blends of sugarcane bagasse and coal: Thermal and kinetic behaviors. **Journal of Thermal Analysis and Calorimetry**, v. 132, n. 2, p. 1333–1345, 2018.

MUMBACH, G. D. et al. Pyrolysis of cocoa shell and its bioenergy potential: evaluating the kinetic triplet, thermodynamic parameters, and evolved gas analysis using TGA-FTIR. **Biomass Conversion and Biorefinery**, v. 12, n. 3, p. 723–739, 1 mar. 2022.

NUMAZAWA, C. T. D. et al. Logging residues and CO2 of Brazilian Amazon timber: Two case studies of forest harvesting. **Resources, Conservation and Recycling**, v. 122, p. 280–285, 1 jul. 2017.

OLIVEIRA, P. R. S. et al. Kinetic and thermodynamic analysis of açaí seeds and insights into bio-oil optimization and composition. **Journal of Thermal Analysis and Calorimetry**, v. 148, n. 23, p. 13427–13439, 2023.

OSMAN, A. I. et al. Physicochemical Characterization and Kinetic Modeling concerning Combustion of Waste Berry Pomace. **ACS Sustainable Chemistry and Engineering**, v. 8, n. 47, p. 17573–17586, 2020.

OZAWA, T. A new method of analyzing thermogravimetric data. **Bull. Chem**, v. 38, n. 11, p. 1881– 1886., 1965.

PRAKASH, S.; ABHISEK, P.; SACHIN, S. Evaluation of kinetic and thermodynamic parameters of Argemone mexicana seed pyrolysis via thermogravimetric analyser. **Biomass Conversion and Biorefinery**, n. 0123456789, 2021.

PROTÁSIO, T. DE P. et al. Insights in quantitative indexes for better grouping and classification of Eucalyptus clones used in combustion and energy cogeneration processes in Brazil. **Biomass and Bioenergy**, v. 143, n. October, 2020.

RAVEENDRAN, K.; GANESH, A.; KHILAR, K. C. Pyrolysis characteristics of biomass and biomass components. **Fuel**, v. 75, n. 8, p. 987–998, 1 jun. 1996.

RIAZ, S.; OLUWOYE, I.; AL-ABDELI, Y. M. Oxidative torrefaction of densified woody biomass : Performance , combustion kinetics and thermodynamics. **Renewable Energy**, v. 199, n. August, p. 908–918, 2022.

RIVERA, J. E. G. et al. Thermogravimetric characteristics and kinetic modeling of Piptocoma discolor pyrolysis and combustion processes to contribute to its use as a renewable energy source in the Ecuadorian Amazon region. **Biomass Conversion and Biorefinery**, v. 13, n. 17, p. 15761–15768, 2023.

SÁ, I. A. et al. Evaluating the quality of wood waste pellets and environmental impact mitigation for decentralized energy recovery in the Amazon. **Renewable Energy**, v. 231, n. February, p. 120929, 2024.

SAHA, D. et al. Pyrolysis kinetics and thermodynamic parameters of plastic grocery bag based on thermogravimetric data using iso-conversional methods. **International Journal of Environmental Science and Technology**, v. 19, n. 1, p. 391–406, 2021.

SAIT, H. H. et al. Pyrolysis and combustion kinetics of date palm biomass using thermogravimetric analysis. **Bioresource Technology**, v. 118, p. 382–389, 1 ago. 2012.

SANTANA, M. A. E.; OKINO, E. Y. A. Chemical composition of 36 Brazilian Amazon forest wood species. **Holzforschung**, v. 61, n. 5, p. 469–477, 1 ago. 2007.

SANTOS, V. O. et al. Pyrolysis of acai seed biomass : Kinetics and thermodynamic parameters using thermogravimetric analysis. **Bioresource Technology Reports**, v. 12, n. August, p. 100553, 2020.

SANTOS, V. O. et al. Analysis of thermal degradation of peach palm (Bactris gasipaes Kunth) seed using isoconversional models. **Reaction Kinetics, Mechanisms and Catalysis**, v. 135, n. 1, p. 367–387, 2022.

SANTOS, V. O. et al. Non-isothermal kinetics evaluation of buriti and inaja seed biomass waste for pyrolysis thermochemical conversion technology. **Biomass Conversion and Biorefinery**, v. 13, n. 12, p. 10893–10909, 2023.

SCOTT, S. A. et al. An algorithm for determining the kinetics of devolatilisation of complex solid fuels from thermogravimetric experiments. **Chemical Engineering Science**, v. 61, n. 8, p. 2339–2348, abr. 2006.

SENUM, G. I.; YANG, R. T. Rational approximations of the integral of the Arrhenius function. **Journal of Thermal Analysis**, v. 11, n. 3, p. 445–447, 1977.

SEO, M. W. et al. Recent advances of thermochemical conversieon processes for biorefinery. **Bioresource Technology**, v. 343, n. October 2021, p. 126109, 2022.

SFB; IPAM. Florestas Nativas de Producao Brasileiras. n. 1, p. 10–27, 2011.

SHI, X.; WANG, J. A comparative investigation into the formation behaviors of char, liquids and gases during pyrolysis of pinewood and lignocellulosic components. **Bioresource Technology**, v. 170, p. 262–269, 2014.

SIDDIQI, H. et al. In-depth physiochemical characterization and detailed thermo-kinetic study of biomass wastes to analyze its energy potential. **Renewable Energy**, v. 148, p. 756–771, 2020.

SILVEIRA, E. A. et al. A hybrid optimization approach towards energy recovery from torrefied waste blends. **Renewable Energy**, v. 212, n. May, p. 151–165, 2023.

SILVEIRA, E. A. et al. Effect of torrefaction severity on the energy recovery from amazonian wood residues for decentralized energy conversion systems. **Biomass and Bioenergy**, v. 193, n. March 2024, 2025.

SINGH, R. K. et al. Pyrolysis of banana leaves biomass: Physico-chemical characterization, thermal decomposition behavior, kinetic and thermodynamic analyses. **Bioresource Technology**, v. 310, p. 123464, 1 ago. 2020.

SONG, F. et al. Novel Insights into the Kinetics, Evolved Gases, and Mechanisms for Biomass (Sugar Cane Residue) Pyrolysis. **Environmental Science and Technology**, v. 53, n. 22, p. 13495–13505, 2019.

STARINK, M. J. A new method for the derivation of activation energies from experiments performed at constant heating rate. **Thermochimica Acta**, v. 288, n. 1–2, p. 97–104, 1996.

TEH, J. S. et al. Thermal analysis technologies for biomass feedstocks: A state-of-the-art review. **Processes**, v. 9, n. 9, 2021.

VÁRHEGYI, G. et al. Thermogravimetric study of biomass pyrolysis kinetics. A distributed activation energy model with prediction tests. **Energy Fuels**, 2010.

VASUDEV, V.; KU, X.; LIN, J. Pyrolysis of algal biomass: Determination of the kinetic triplet and thermodynamic analysis. **Bioresource Technology**, v. 317, n. August, p. 124007, 2020.

VYAZOVKIN, S. **ADVANCED ISOCONVERSIONAL METHODJounal of Thermal Analysis**. [s.l: s.n.].

VYAZOVKIN, S. et al. Thermochimica Acta ICTAC Kinetics Committee recommendations for performing kinetic computations on thermal analysis data. **Thermochimica Acta**, v. 520, n. 1–2, p. 1–19, 2011.

VYAZOVKIN, S. Misinterpretation of Thermodynamic Parameters Evaluated from Activation Energy and Preexponential Factor Determined in Thermal Analysis Experiments. **Thermo**, v. 4, n. 3, p. 373–381, 2024.

WANG, S. et al. Lignocellulosic biomass pyrolysis mechanism: A state-of-the-art review. **Progress in Energy and Combustion Science**, v. 62, p. 33–86, 2017.

WELFLE, A. Balancing growing global bioenergy resource demands - Brazil's biomass potential and the availability of resource for trade. **Biomass and Bioenergy**, v. 105, n. 2017, p. 83–95, 2017.

WHITE, J. E.; CATALLO, W. J.; LEGENDRE, B. L. Biomass pyrolysis kinetics: A comparative critical review with relevant agricultural residue case studies. **Journal of Analytical and Applied Pyrolysis**, v. 91, n. 1, p. 1–33, 2011.

WILD, P. J. DE; WOUTER J. J. HUIJGEN; RICHARD J.A. GOSSELINK. Lignin pyrolysis for profi table lignocellulosic biorefi neries. **Biofuels, Bioproducts and Biorefining**, v. 8, n. 6, p. 743, 2014.

XU, X.; PAN, R.; CHEN, R. Combustion Characteristics, Kinetics, and Thermodynamics of Pine Wood Through Thermogravimetric Analysis. **Applied Biochemistry and Biotechnology**, v. 193, n. 5, p. 1427–1446, 2021.

YAO, F. et al. Thermal decomposition kinetics of natural fibers: Activation energy with dynamic thermogravimetric analysis. **Polymer Degradation and Stability**, v. 93, n. 1, p. 90–98, 2008.

ZHUANG, X. et al. Synergistic effects on the co-combustion of medicinal biowastes with coals of different ranks. **Renewable Energy**, v. 140, p. 380–389, 2019.